Wave and wind conditions in the Red Sea
A numerical study using a third generation wave model

by

Ahmed Mohamed Elfatih Saad

A thesis submitted in partial fulfillment for the
degree of Master in Physical Oceanography
in the

Geophysical Institute
University of Bergen

June 2010

UNIVERSITY OF BERGEN

Geophysical Institute
University of Bergen

Master in Physical Oceanography

by

Ahmed Mohamed Elfatih Saad

Abstract

In order to understand how waves behave and how other parameters can interact between ocean and atmosphere we can use a numerical model. For the Red Sea basin wave measurements are absent and due to that a WAM wave model is used to study the wave climate.

The aim of this thesis is to run a wave model for the Red Sea area to begin a local forecast service and then estimate climatology of wave height, needed in almost all coastal engineering studies. As well as to give engineers a description of ocean surface waves and forces, this knowledge about Red Sea wave conditions can help the local fishermen that use small vessels. The third generation wave model WAM is used to hindcast the wave condition in the Red Sea for the year 2007. The WAM model is forced using wind data obtained from the European Centre for Medium-Range Weather Forecasts (ECMWF).

Acknowledgements

I am very grateful to my supervisor Dr. Knut Barthel and to my co-supervisor Dr.Øyvind Breivik for the privilege of having excellent guidance and constant support during this work. My knowledge has benefited greatly from his expertise, enthusiasm and encouragement. I also wish to express my warmest gratitude my co-supervisor Dr.Øyvind Breivik for the numerous invaluable suggestions during this work and for giving valuable suggestions to the manuscript. I also thank the administration staff at the geophysics institute. I am enormously grateful to the Norad's Programme for Master Studies (NOMA) for the support during my master study.

The 50% of the main body of this work was carried out at the Geophysical Institute ($GFI, Norway$). and the other 50% of this work was carried out at Institute of Marine Research ($IMR, Sudan$), I thank the staff, researchers and employees at these institutes for the comfortable working environment and excellent facilities for this work.

Especially warm thanks go to my parents Wedad and M.Elfatih, my fiancee Hiba, my family, and to all my friends for their constant support and patience during this work.

Ahmed M.Elfatih Saad
Bergen - June 2010

Contents

List of Figures

to my

parents WEDAD and M.ELFATIH, and to my Love

with my love

Chapter 1

Introduction

1.1 Motivation

Ocean waves are the result of forces acting on the ocean, the gravity of the Earth, pressure from the atmosphere, earthquakes, and the Coriolis force due to the Earth's rotation. One of the most distinctive phenomena on the surface of the oceans is the phenomenon of wave generation by wind; they play significant part in both climate and society by affecting offshore projects and fishing industry. Wind waves have a frequency range of 1-30 seconds and are not deflected by the Earth's rotation. The growth of wind waves is controlled by the wind speed, wind duration and the fetch, *where fetch is the transport distance of the wind over the water body.* For more information about swell see chapter 2 section 2.3. In this thesis we deal with wind waves. Ocean gravity waves can be found thousands of kilometers away from the places they were generated [21]. The study of the wave conditions and the forces they generate in both offshore and coastal regions is an essential prerequisite for the design of many near shore projects. And in the long term waves determine the geometry of beaches. Reliable data on the wave characteristics can be derived from long-term extensive wave measurements, or extended wave hindcast using numerical wave models.

The main purpose of a wave model is to make hindcasts and forecasts of the sea state, and this can be used for many applications such as ship routing, offshore industries and fishing. The WAM model is a spectral wave prediction model that solves and describes the evolution of the energy balance equation for the two dimensional wave spectrum [9]. The WAM model has been in operational use since 1992, and today it is used by more than 100 institutes all over the world [9]. In

collaboration with the Meteorological Institute in Bergen WAM was set up and run for the Red Sea. The Red Sea is one of the most unexplored areas of the Northern Hemisphere oceans, so it is interesting to run the WAM model for this area to extract more knowledge and information about the wave conditions there [11].

1.2 Description of the Red Sea

1.2.1 Geography

The Red Sea is a semi-enclosed tropical body of water and it is an arm of the Indian Ocean and a major shipping route. It is located between the Arabian Peninsula and Africa, in one of the hottest, driest regions on Earth. The Red Sea has a total coastline of about 4000 km that lies between latitudes 12^oN and 30^oN and has total surface area of roughly 438,000 km^2. Length is about 1,930 km; and it is bordered by Egypt, Sudan[1], Eritrea and Djibouti on the west, and Yemen and Saudi Arabia on the east.

The coastlines of the Red Sea are remarkably straight and parallel for nearly 500 km south of the Gulf of Suez to about 24^oN with a separation of 190 km. And south of there, the coastlines become more sinuous, and the sea gradually widens to a maximum width of 350 km between 16^oN and 17^oN before narrowing to about 18 km at the Straits of Bab el Mandab. Irregular, eroded escarpments face seaward from the uplifted rift shoulders that flank the Red Sea [2]. The Red Sea has three distinct zones of depth; the shallow reef studded shelves of less than 50m, the deep shelves of 500 - 1000 m. and the central trench of more than 1000 m. The maximum depth of the Red Sea is 3040 m off Port Sudan, See Figure 1.1.

The strait of Bab Al Mandeb separates the Red Sea from the Indian Ocean via the Gulf of Aden. In the north the Red Sea ends into two gulfs, the deep Gulf of Aqaba and the shallow Gulf of Suez, which is connected to the Suez Canal.

[1]Sudan has a total coastline of about 750 km.

Much of the coast is bordered by fringing reefs that are about 10 km wide and a few meters deep [32].

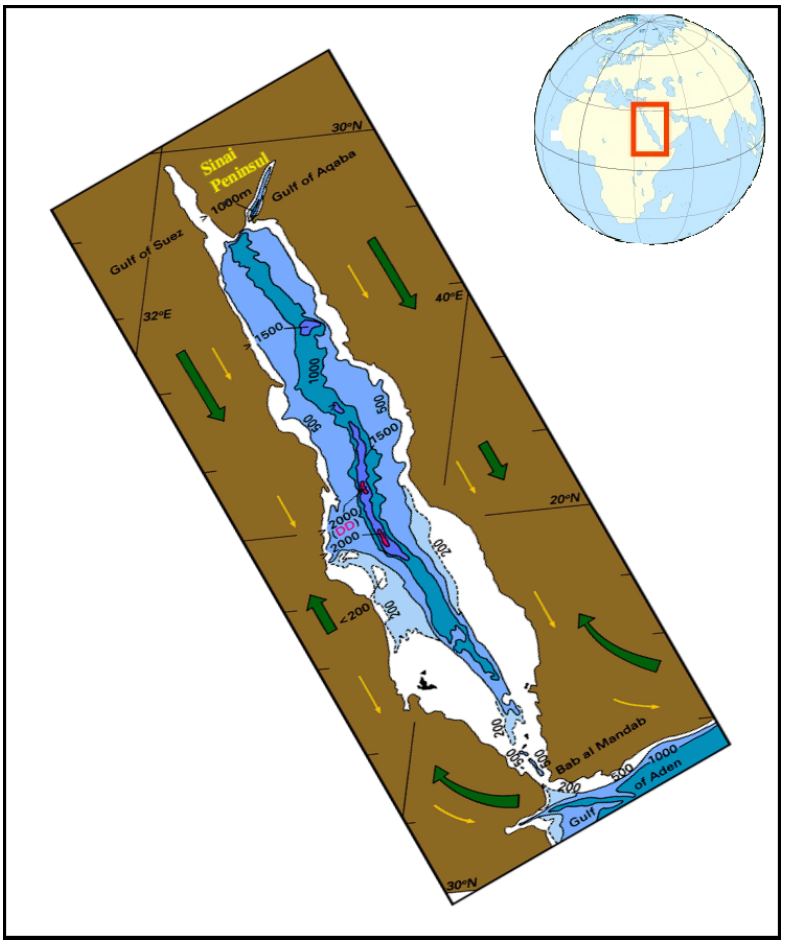

FIGURE 1.1: Shows bathymetric map of the Red Sea [32].

1.2.2 Climate

The weather in the Red Sea area is extremely hot and arid in the summer. The southern part of the Red Sea is considered to be among the hottest areas in the world [32]. Water circulation in the Red Sea is driven by monsoonal wind patterns. Monsoon winds occur because of the different heating between the land surface and sea in the Indian ocean and Asia. In the north a northwesterly monsoon is controlled by the eastern Mediterranean weather systems. In the winter season or monsoon, most of the wind in the Southern Red Sea is from the south and this wind is controlled by the Indian monsoon system. It reverses from southeast

TABLE 1.1: **Red Sea Fact sheet**

Area	**Fact**	**Fact in number**
Red Sea	Total surface area	438,000 km^2
	Length	1930km
	Average width	350km
	Maximum depth	3040m
Gulf of Aqaba	Length	160 km
	Maximum depth	1850 m
	Width	24 km
Bab Al Mandab Strait	Average depth	300 m
	Narrowest width	18 km
	Sill depth	137 m
Gulf of Suez	Length	300 km
	Range depth	55-73 m

* For more information check [6],[4].

during winter (October to May) to northwest during summer (June to September) [11], see Figure 1.2 and Figure 1.3. In the summer monsoon, the wind in the Red Sea blows from the north, causing a surface current out of the Red Sea [29]. See Figure 1.2 (b).

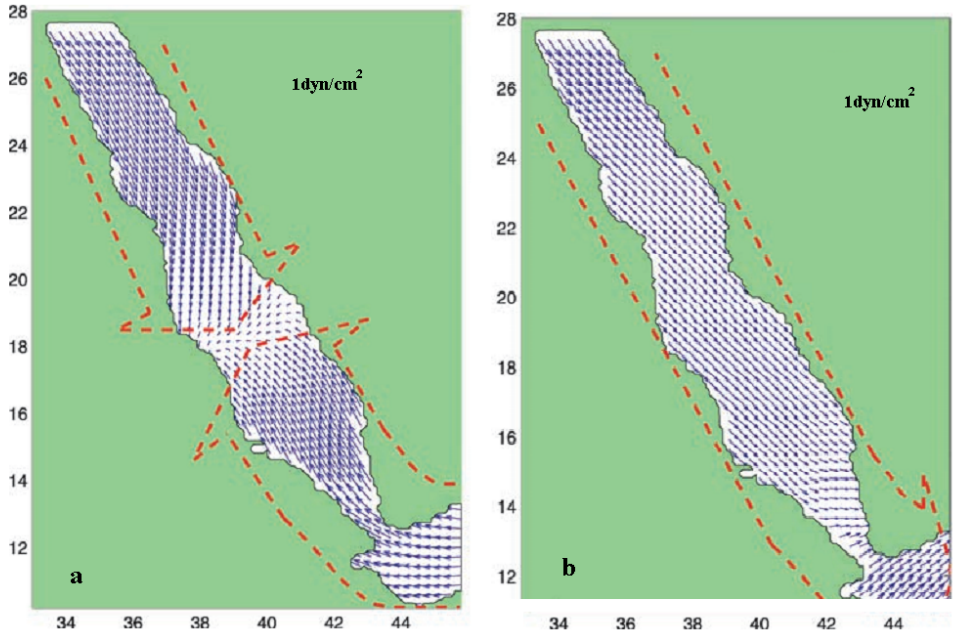

FIGURE 1.2: Wind-stress fields for (a) January and (b) July [11].

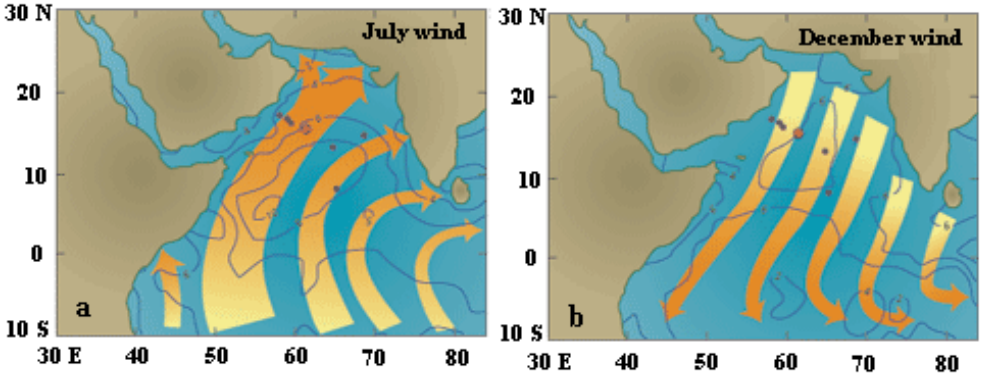

FIGURE 1.3: Monthly mean wind stress, during winter (December) and summer (July) as described in Honjo and Weller [31]

.

Chapter 2

Theory

2.1 Wave Theory

Waves are used to describe the vibration or disturbance which transfer from one point to another through a medium without giving the medium any displacement of the particles of the medium. The shape of a wave is given by its amplitude which can change in space and time, phase, wavelength and frequency [19].

Earthquakes or big ships can create waves; but the most common cause is wind. As wind blows over the water surface friction will force it to ripple. The strength of the wind, the distance the wind blows - called fetch- and the length of the gust can determine how big the ripples will become. Waves are divided into several parts, see Figure 2.1. The crest is the highest point on a wave, while the trough or valley between two waves is the lowest point. Wavelength is the horizontal distance, either between the crests or troughs of two consecutive waves. Wave height (H) is the vertical distance between a wave's crest and the next trough. Wave period (T) measures the length of the wave in time. A wave period (T) can be measured by picking a stationary point and counting the seconds it takes for two consecutive crests or troughs to pass it [18]. The frequency, f, is the number of crests which pass a fixed point in 1 second. It is usually measured in numbers per second ($Hertz$) and is the same as $1/T$. The rate of propagation, c, is the speed at which the wave profile travels, i.e. the speed at which the crest and trough of the wave advances. It is commonly referred to as wave speed or phase speed. The steepness of a wave is the ratio of the height to the length H/λ.

Some physical assumptions concerning sea water are often being made :

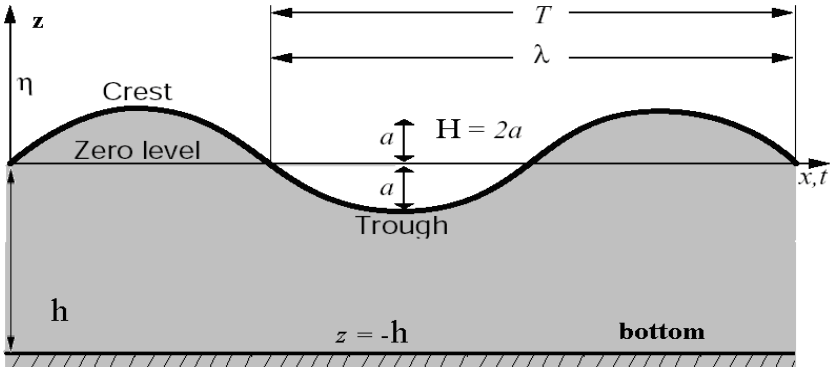

FIGURE 2.1: Basic parameters used to describe a wave.

- The water is incompressible and that means the density ρ_w is constant:

$$\frac{1}{\rho_w}\frac{d\rho_w}{dt} = 0 \tag{2.1}$$

Thus, the continuity equation

$$\frac{1}{\rho_w}\frac{d\rho_w}{dt} + \left[\frac{\partial u}{\partial x} + \frac{\partial v}{\partial y} + \frac{\partial w}{\partial z}\right] = 0 \tag{2.2}$$

Reduces to

$$\vec{\nabla} \cdot \vec{u} = 0 \tag{2.3}$$

- The water is an inviscid fluid, and that means the only forces acting on the water are pressure forces acting perpendicular to the surface. Friction is ignored, so the viscosity:

$$\mu_w = 0 \tag{2.4}$$

- The water fluid is irrotational.

$$\vec{\nabla} \times \vec{u} = 0 \tag{2.5}$$

And that means the flow can be given by a velocity potential ϕ:

$$\vec{u} = \vec{\nabla}\phi \tag{2.6}$$

By Eq.(2.1) and Eq.(2.6) we get the equation:

$$\vec{\nabla} \cdot \vec{\nabla}\phi = 0 \tag{2.7}$$

In $x - z$ coordinates this gives the Laplace equation

$$\frac{\partial^2 \phi}{\partial x^2} + \frac{\partial^2 \phi}{\partial z^2} = 0 \tag{2.8}$$

Now with the linearized boundary conditions at z = 0

$$\frac{\partial \phi}{\partial z} = \frac{\partial \eta}{\partial t} = w \tag{2.9}$$

The linearized form of the unsteady Bernoulli equation is

$$\frac{\partial \phi}{\partial t} + \frac{p}{\rho} + gz = 0 \tag{2.10}$$

If we apply the surface boundary condition $p = 0$ at $z = \eta$ to the Eq.(2.10) and for small amplitude waves the term $\frac{\partial \phi}{\partial t}$ can be evaluated at z=0 rather than at $z = \eta$, [25] giving

$$\frac{\partial \phi}{\partial t} = -g\eta \tag{2.11}$$

At the flat bottom where $z = -h$:

$$\frac{\partial \phi}{\partial z} = w = 0 \tag{2.12}$$

We have to solve Eq.(2.8), and apply the boundary conditions. We assume

$$\eta(x, t) = a \ sin(kx - wt) \tag{2.13}$$

Eq.(2.13) is a component of the wave profile where $k = 2\pi/\lambda$ is the wave number and $w = 2\pi/T$ the angular frequency. Eq.(2.13) gives a fair representation in ocean wave physics and it contains spatial and temporal coordinate that can describe the surface displacement at a fixed point, x =const, varying in time and at a certain time, t = const, varying in space.

The variation of wave speed with the wavelength is called dispersion and the functional variation of angular frequency/phase speed with the wave number is called dispersion relation [25]. So by inserting Eq.(2.13) into Eq.(2.8) and applying the boundary conditions the dispersion relation becomes

$$w^2 = gk \ \tanh \ kh \tag{2.14}$$

Like all truly periodic waves, Eq.(2.13) yields the relation:

$$\lambda = cT = c/f \tag{2.15}$$

Where c is the wave speed, so it can be written as λ/T or ω/k. The wave speed is related to the wave number by

$$c = \sqrt{\frac{g}{k}\tanh \ kh} = \sqrt{\frac{g\lambda}{2\pi}\tanh \ \frac{2\pi h}{\lambda}} \tag{2.16}$$

Where g is acceleration due to gravity, "tanh" is the hyperbolic tangent and h is the water depth.

For the short waves in deep water waves $\lambda < 2h$,

$$\tanh\frac{2\pi h}{\lambda} = \tanh \ kh \simeq 1 \tag{2.17}$$

Then

$$c_s = \sqrt{\frac{g\lambda}{2\pi}} = \sqrt{\frac{g}{k}} \tag{2.18}$$

For long or shallow water waves $\lambda > 20h$,

$$\tanh\frac{2\pi h}{\lambda} = \tanh\ kh = kh \tag{2.19}$$

Then

$$c_l = \sqrt{gh} \tag{2.20}$$

See Figure 2.2

A gravity wave may be represented as a sinusoidal movement as shown in Figure 2.1. It is the gravity that forces the surface back to its original level when for example the wind has caused a displacement away from the mean surface level [21]. The result is an oscillating motion where kinetic energy is transformed into potential energy and back again as the wave propagates. The ordinary gravity wave has a wave period between 1 and 30 seconds [21], See Figure 2.3.

We can regard the sea surface as a sum of many different sinusoidal waves. It can be compared with a huge column with many layers on top of each other where every layer represents one wave. See Figure 2.4.

2.2 The orbital motion of water particles beneath waves

The orbital motion of water particles beneath waves is a famous phenomenon which is seen just by monitoring surfers . If we watch any floating object, it moves up the front to the wave crest and then will be moved down to its trough. The bigger the wave the larger the orbit. In deep water, when the sea bottom is deeper than the wave base [1] the water particles have almost the same displacement in the horizontal as in the vertical plane, making close to perfect circles. However, waves

[1] Wave base is where the water depth is equal to about one half the wavelength [22].

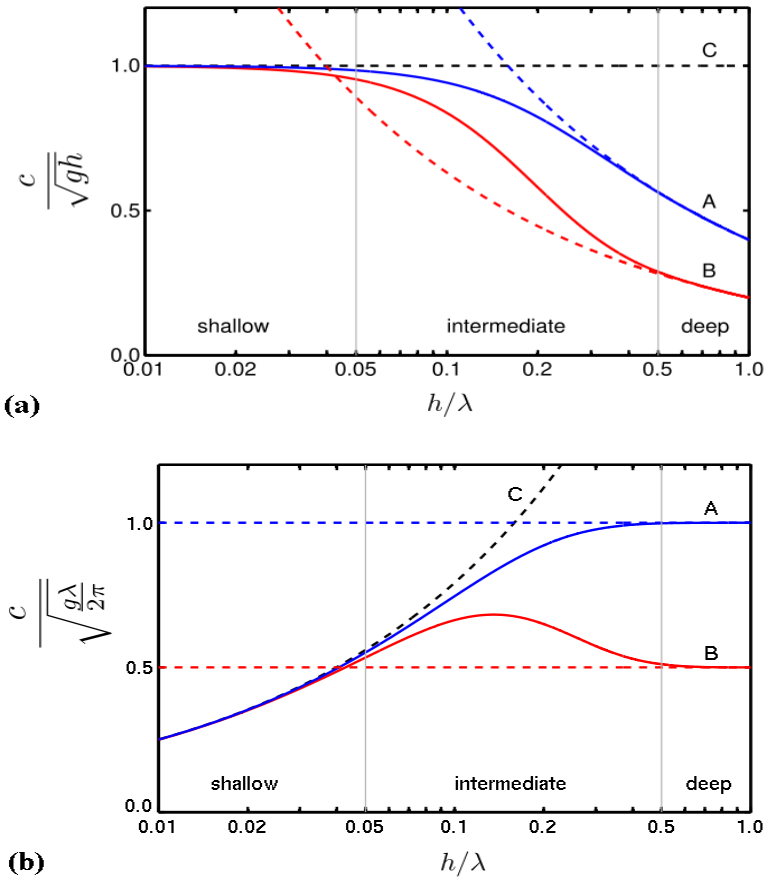

FIGURE 2.2: Dispersion of gravity waves on a fluid surface. In (a) is shown how the phase and group velocity divided by the shallow water velocity depends on the relative depth h/λ. In (b) is shown how the phase and group velocity divided by the deep water , phase velocity depends on the relative depth h/λ. Blue lines (A): phase velocity; Red lines (B): group velocity; Black dashed line (C): phase and group velocity $\sqrt{gh}$ valid in shallow water. Full lines: dispersion relation valid in arbitrary depth. Dashed lines (blue and red): deep water limits [3].

that are in water shallower than the wave base will start to feel the bottom and interact with the ocean floor, making the motion becomes elliptic, see Figure 2.5. It is apparent that only the energy follows the wave, not the water particles. In shallow water the displacements are much larger in the horizontal than in the vertical plane. In deep water the orbits decrease exponentially with depth, only affecting the top layer down to the wave base of the water column.

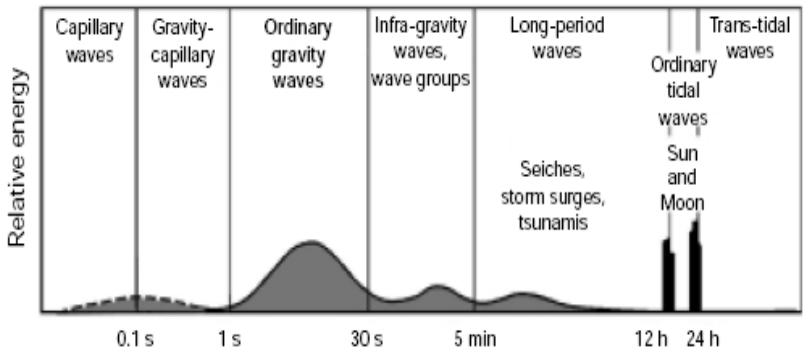

FIGURE 2.3: Wave energy in the ocean as a function of wave period [21].

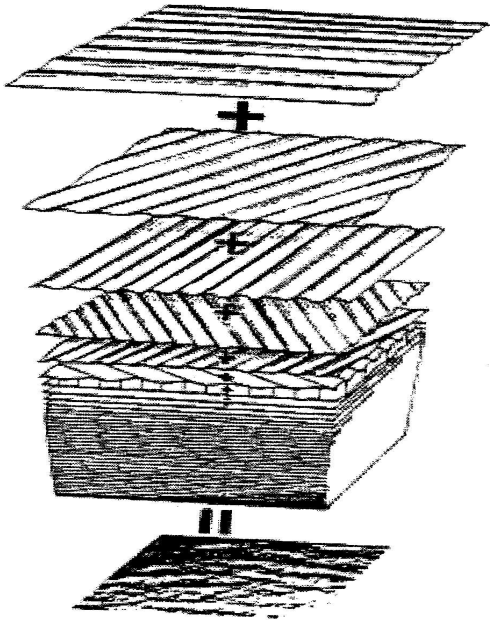

FIGURE 2.4: The column of layers where each layer represents a sinusoidal wave [33].

The orbital path of a water particle covers a circumference of πh during one period, which equals a velocity of $\pi h/T$. This corresponds to the maximum velocity in the vertical as well as the horizontal plane. If we compare this formula to the phase speed in Eq.(2.15), we see that the particle velocity is small as λ in deep water most often is substantial in comparison to πh. In reality the orbits of wave particles are not completely closed, the orbital motion reduces with depth and that means they move slower in the horizontal plane with depth. And this

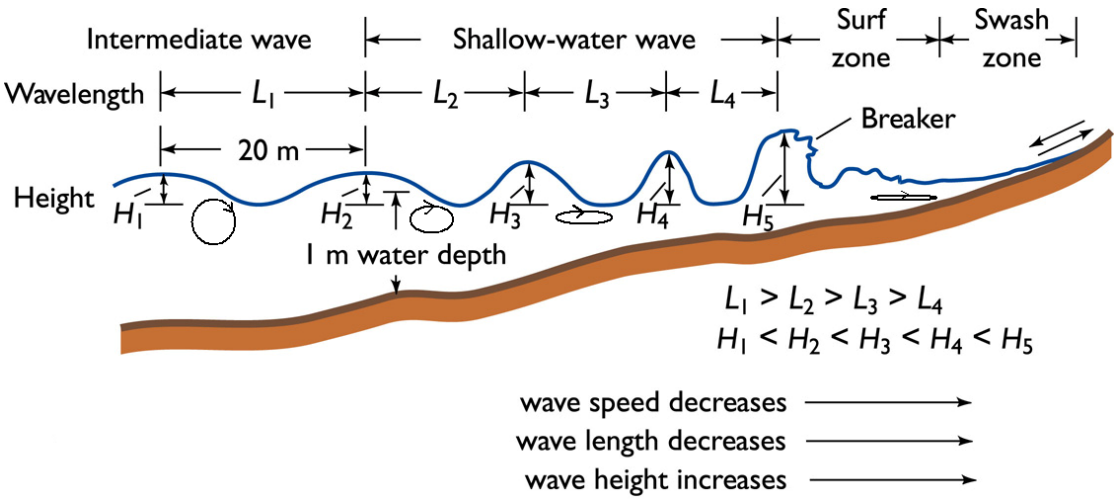

FIGURE 2.5: Shows the process of breaking, energy dissipation by bottom friction. As waves pass from deep water onto shallow water, the waves become highly nonlinear [22].

creates a slight forward movement in the direction of the wave, known as the Stokes drift. Figure 2.6.

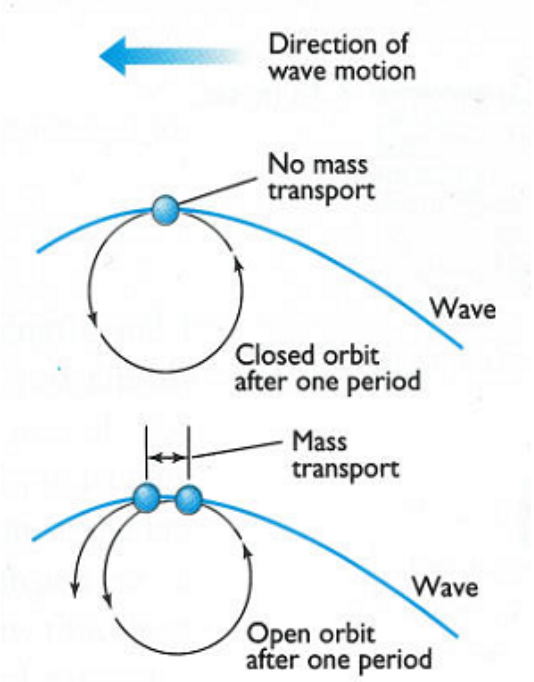

FIGURE 2.6: Path shift of a water particle during two wave periods, Stokes drift [22].

2.3 Wind sea and swell

The waves which are directly connected to the wind are often called wind sea. When waves propagate away from where they were generated and no longer are affected by the wind forcing that created them, they are called swell (the wind does not longer transport energy into the waves).

It is important in coastal practice to differentiate between those two types of surface waves. Wind sea refers to short-period waves still being created by winds. Swell refers to waves that have moved out of the generating area. The greater the fetch is, the larger the waves become until they reach an equilibrium state, the fully developed wind sea. In general, swells are more regular waves with well-defined long crests and relatively long periods [23]. Swell can not only carry forward a great amount of energy, but also transport momentum. One can believe that, because of the energy transport, voluminous amount of water would also be transported, but this is not the case. One single water particle does not have a big forward movement, actually it is a very small motion [22].

2.4 Wave groups

Despite each wave component is propagating at its own phase speed, the group as a coherent unit moves at the same speed, the group speed which is expressed by :

$$c_g = \frac{d\omega}{dk} = \frac{c}{2}\left(1 + \frac{2kh}{\sinh 2kh}\right) \tag{2.21}$$

Where c is given by Eq.(2.16).
The group velocity c_g is the velocity at which energy is transfered along a group of waves [21].

[2] For short waves in deep water, when h $> \frac{\lambda}{2}$ so that $kh > \pi$, we get

[2]Eq.(2.22) is valid only for short waves in deep water.

$$c_{gs} = \frac{c_2}{2} = \frac{1}{2}\sqrt{\frac{g}{k}}. \tag{2.22}$$

Where as for long waves in shallow water, where $\lambda > 20h$ so that $kh < \frac{\pi}{10}$, we get

$$c_{gl} = c_l = \sqrt{gh} \tag{2.23}$$

2.5 Wave Refraction

One of the most noticeable features of wave crests entering shallow water at an angle is *wave refraction*. These lines do not break simultaneously because different parts of the wave crest are in different depths of water. Waves are affected by the depth, they change as they begin to feel the bottom, in the way that waves moving towards the coast at some angle arrange this crests parallel to the shoreline. See Figure 2.7.

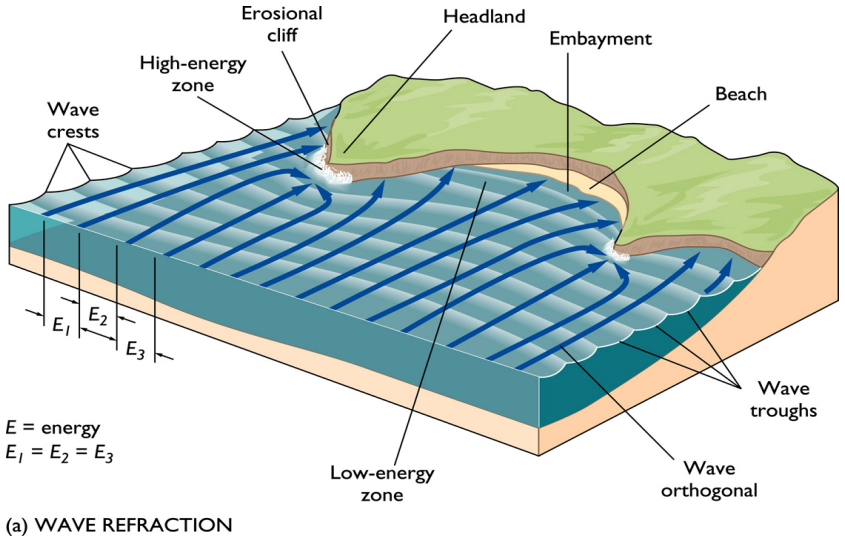

FIGURE 2.7: Diagram shows the pattern of wave refraction along an irregular shoreline [22].

2.6 The wave spectrum

The surface looks like it is composed of random waves of various wavelengths and periods, and when we try to describe the sea surface we can make some simplification that leads to the concept of the spectrum of ocean waves [8]. The wave spectrum can describe the wave energy of different wave-lengths and wave frequencies on the sea surface.

By Fourier analysis a wave record of sea surface can be decomposed into a large number of sinusoidal waves of different frequencies, directions, amplitudes and phases. And each frequency describes a wave component, and each component has an associated amplitude and phase.

$$\eta(t) = \eta_0 + \sum_{j=1}^{N} a_j sin(j\omega_0 t + \phi_j) \tag{2.24}$$

Notation used in Eq.(2.24)

$\eta(t)$	surface elevation at time t.
η_0	mean surface level .
ω_0	angular frequency of the longest wave component fitted to the record.
j	Wave component number.
N	total number of components.
ϕ_j	phase angle of the jth component.
a_j	amplitude of the jth component.

The high frequency components have less energy. The sum of squares of the amplitudes, a_j^2, is the variance [3] of the surface elevation η. If we take the square of the amplitude of each wave component and plot it against its frequency, we will obtain the variance spectrum, $S(f)$. However, more often the variance density spectrum, $E(f)$, is being used, which represents the squared amplitude of the spectral component divided by the width of the frequency interval it represents [21]. Figure 2.8 shows a typical spectrum of a wave system.

[3]The variance of a wave record is obtained by averaging the squares of the deviations of the water surface elevation, η from its mean η_0 [21].

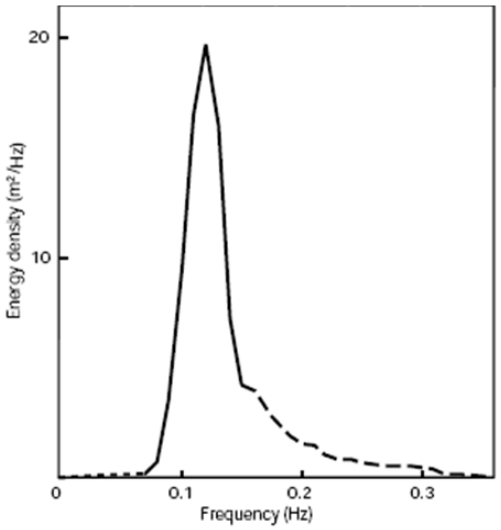

FIGURE 2.8: An example of a wave spectrum [21].

There are many ways to calculate the wave spectra by using different measuring techniques, but the most commonly used algorithm is the fast Fourier transform. The wave spectrum can be obtained using numerical models, either given in one dimension ($1D$) *the frequency spectrum* - and this represent the total sea state -, or in two dimensions ($2D$) *the directional frequency spectrum* - representing one spectrum per directional sector [21].

2.7 Model forms

The modeling of sea state is in most cases described by the concept of a wave spectrum [14]. Models can describe the spectrum in some functional form, usually in terms of frequency, $E(f)$, frequency and direction $E(f, \Theta)$, or wave number $E(k)$ [21].

The ***Pierson-Moskowitz spectrum*** [17] defines a parametric model for a fully developed wind sea based on observations recorded with the shipborne wave recorder on board British ocean weather ships during a five year period 1955-1960 [17]. They considered constant winds blowing without limited fetch or duration.

Then the spectrum reaches equilibrium. The original form of this model spectrum is:

$$E(f) = \frac{\alpha g^2}{(2\pi)^4 f^5} e^{\left[-0.74\left(\frac{g}{2\pi u f}\right)^4\right]} \tag{2.25}$$

Notation used in Eq.(2.25)

$E(f)$	is the variance density $(m^{-2}s)$
f	frequency (Hz)
u	the wind speed (ms^{-1}) at 19.5 m above the sea surface
g	the acceleration due to gravity (ms^{-2})
α	a dimensionless quantity, $\alpha = 0.0081$.

From the above parameters the peak frequency of the Pierson-Moskowitz spectrum is:

$$f_p = 0.877 \frac{g}{2\pi u} \tag{2.26}$$

Figure 2.9 shows fully developed wave spectra measured for various wind speeds.

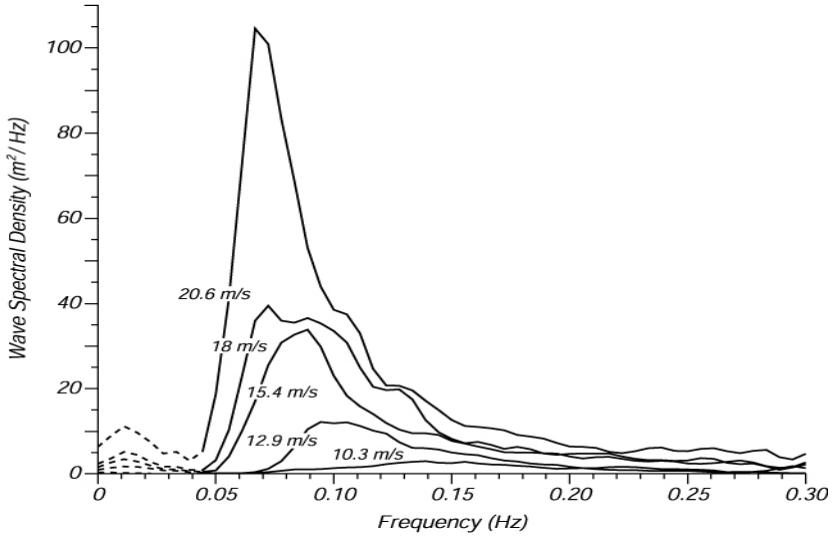

FIGURE 2.9: Wave spectra of a fully developed sea for different wind speeds according to Moskowitz (1964) [17].

Many parameters can be derived from the spectrum similar with any statistical distribution. The nth order moment[4], m_n is defined by:

$$m_n = \int_0^\infty f^n E(f)\, df \tag{2.27}$$

From Eq.(2.25) and Eq.(2.27) we can calculate the significant wave height, H_{m_0} for fully grown sea:

$$H_{m_0} = 0.0246u^2 \tag{2.28}$$

Where H_{m_0} is given in meter and u in ms^{-1}.

Eq.(2.26) and Eq.(2.28) are valid for fully developed sea only [9]. The ***Pierson-Moskowitz spectrum*** does not apply for waves in the growing phase where fetch or duration are limiting factors. The ***JONSWAP spectrum*** is an updated and extended version of the ***Pierson-Moskowitz spectrum***. Observations made by Hasselmann et al. during the Joint North Sea Wave Project (JONSWAP), were analyzed and lead to a description of wave spectra growing in fetch limited condition. The model has been used extensively in ocean surface wave studies [14].

The JONSWAP spectrum formula is expressed as:

$$E(f) = \frac{\alpha g^2}{(2\pi)^4 f^5} e^{\left[-1.25\left(\frac{f}{f_p}\right)^{-4}\right]} \gamma(f) \tag{2.29}$$

The function γ is the peak enhancement factor, which modifies the interval around the spectral peak making it much sharper than in the Pierson-Moskowitz spectrum [21], see Figure 2.10.

[4]"The first moment of a distribution of N observations X_1, X_2, , X_n is defined as the average of the deviations x_1, x_2, , x_n from the given value X_0. The second moment is the average of the squares of the deviations about X_0; the third moment is the average of the cubes of the deviations, and so forth. When X_0 is the mean of all observations, the first moment is obviously zero, the second moment is then known as the *variance* of X and its square root is termed the *standard deviation*" [21].

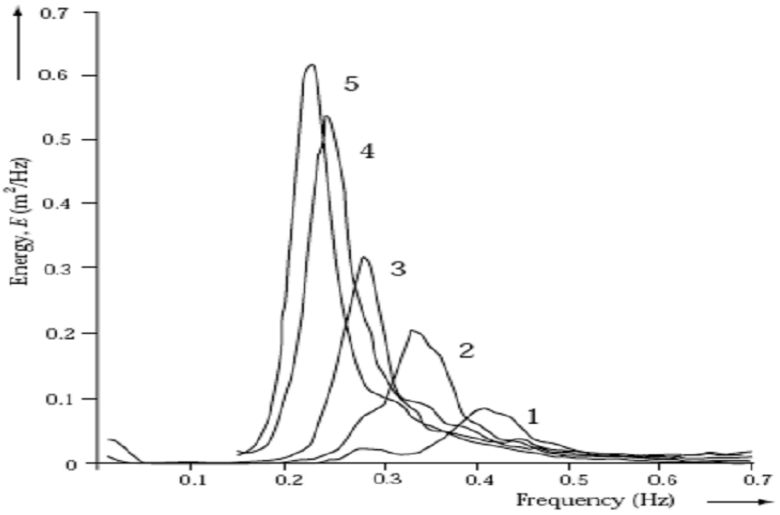

FIGURE 2.10: Wave spectra of a developing sea for different fetches according to Hasselmann et al., (1973) [12].

Chapter 3

Wave Modeling

3.1 The wave energy balance equation

Numerical wave modeling has become essential tools for wave forecast services and wave studies climatology; to help off-shore design criteria; operational planning and marine operations. The first idea and principle of wave modeling were well known in the sixties, but during the years 1960 - 1970 none of the developed wave models could compute the wave spectrum from the full energy balance equation. So to do that they introduced some assumptions to the energy balance equation and they used the basic physical principles that are described in Chapter 2.

Wave models are forced by surface winds. The evolution in time and space of each component of the wave spectrum is calculated using the wave energy balance equation expressed by

$$\frac{\partial E}{\partial t} + \nabla \cdot (c_g E) = S = S_{in} + S_{nl} + S_{ds} \tag{3.1}$$

Where:

$E = E(f, \theta, x, t)$	is spectral wave energy density (surface variance spectrum) depending on wave frequency, f , and wave direction, θ , position, x, and time, t.
$c_g = c_g(f, \theta)$	is the deep-water group velocity.
S	Is the total source function, containing three terms:
	S_{in} energy input by the wind.
	S_{nl} non-linear energy transfer by wave-wave interactions.
	S_{ds} dissipation.

Eq.(3.1) is valid only for deep water with no refraction and no significant currents, and describes the gain, loss, and shifting of energy.

3.1.1 Wind input

Energy is transfered to the wave field through the surface stress exerted by the wind. The square of the wind speed varies roughly as the wave energy, so an error in wind specification can lead to a large error in the wave energy and subsequently in parameters such as significant wave height.
S_{in} is the input by the wind. It is scaled in terms of friction velocity, u_* [15], and is defined as:

$$S_{in} = \beta E \tag{3.2}$$

Where β is wave growth described by:

$$\beta = max\left\{0, 0.25\frac{\rho_a}{\rho_w}\left(28\frac{u_*}{c}cos\Theta - 1\right)\right\}\omega \tag{3.3}$$

$\omega = 2\pi f$, ρ_a and ρ_w is density of respectively air and water, and Θ is the direction of propagation relative to wind direction.
Figures 3.1 and 3.2 shows the three source terms, and how they vary with frequency in two duration limited cases, after 3h *(young wind sea)* and 96 hours *(old wind sea)* respectively, obtained by the WAM model [9]. In these figures the wind input source function is represented by connected open circles, and it is as expected always positive, and the dissipation is always negative, while the nonlinear interactions shift signs. We see how the wind input decreases with duration. Also, the wind input goes into lower frequencies with duration.

3.1.2 Nonlinear interaction

The growth of wind generated waves can be expressed by linear theory as long as waves on average are not very steep, but when the steepness of the wave field

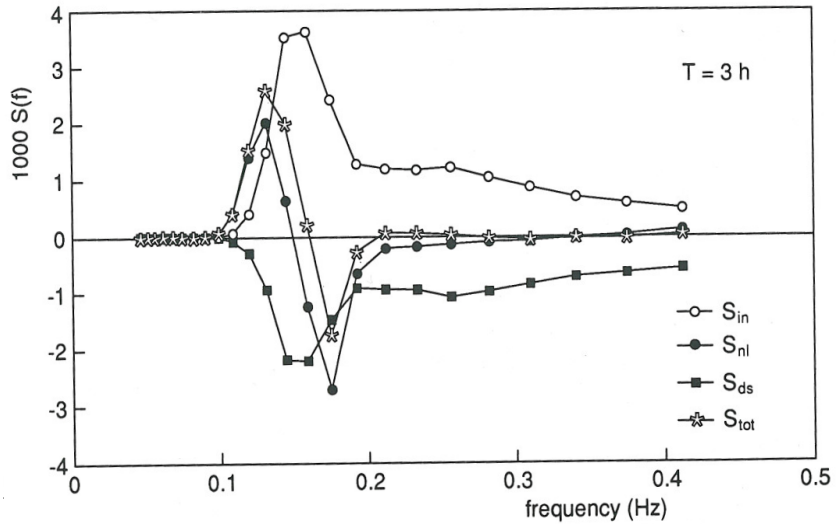

FIGURE 3.1: The energy balance for young duration limited wind sea [9].

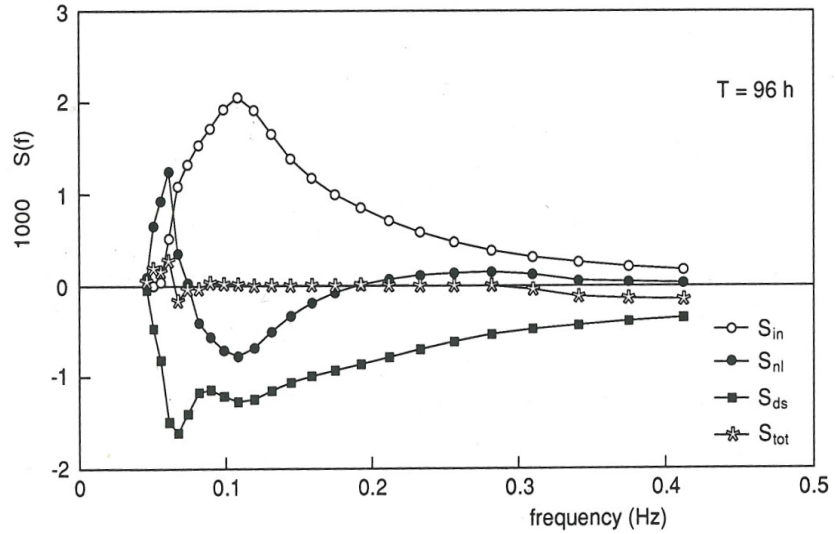

FIGURE 3.2: The energy balance for old wind sea [9].

increases the non-linear processes become more important to the growth of the wave spectrum. The weakly non-linear resonant, wave-wave interaction process is responsible for the transfer of energy along the wave spectrum from higher to lower frequencies [21]. In Figure 3.1 the non-linear interaction is given by the filled circles, and the total transfer by the asterisk.

For young sea, see Figure 3.1, we see at low frequencies the positive lobe of the total transfer centered to the left of the peak frequency. This creates the down-shift of the spectrum observed in developing seas, while in the energy balance for

old wind sea, Figure 3.2, this lobe centered closer to the peak of frequency giving much weaker downshift.

3.1.3 Dissipation

Surface gravity waves suffer attenuation through different processes of energy dissipation :

- bottom friction:
  Is the most important wherever the water depth is less than half a wavelength so that the wave motion will change near the bottom, see Figure 2.5.
- internal processes:
  By viscosity acting throughout the water column and also in the surface by white capping. Here, the emphasis will be on deep water where bottom interaction is negligible [10].

The dissipation of energy by viscous processes is known to be important for wavelengths in the capillary region. However, most energy loss in deep water is due to white capping of breaking waves.
From Figure 3.1 and Figure 3.2 we see how the dissipation change with wave duration or wave age (black squares), and Figure 3.1 shows how the dissipation is just like the mirror of the wind input after 3 hours, only slightly weaker. But in Figure 3.2 we see that the effect is reduced because the sea state is getting closer to its saturation state [20].

3.2 Brief historical perspective on wave modeling

The first numerical wave model was developed by Gelci et al [13].
Spectral wave models solve the wave energy balance equation with its corresponding source terms. The three generations developed are similar, the main difference being how to parameterize the source functions and the computation of the nonlinear interaction [9].

3.3 The Red Sea WAM model

Set-up/Grid and boundary conditions

WAM can be set up and run for any given area, regional or global grid, with a prescribed topographic dataset. The grid resolution can be arbitrary in space and time. Also, the division of the frequency and wave direction can be prescribed by the user. The model outputs the significant height of wind waves and swell, primary wave direction, secondary wave direction, primary wave mean period, secondary wave mean period, direction of swell waves, significant height of swell waves, mean period of swell waves, wind direction, wind speed, direction of wind waves and significant height of wind waves. Two dimensional spectra are also available from selected locations.

The WAM-model is dependent of the wind speed at a height of 10 m covering the modeled area. A historical dataset of winds are used to force the wave forecast model every three hours. The model was set-up for the Red Sea, for a domain bounded by the parallels 30^oN and 12^oN and by the meridians 32^oE and 44^oE. The model domain was assumed to be closed with no wave energy exchange with the open ocean. The topography data are taken from the Earth Topography Two Minutes Grid (ETOPO2) database at a resolution of 2 minutes of latitude and

longitude.

From this topography data base an interpolation to the different grid points was done using the pre-processing tools of met.no (Norwegian Meteorological Institute). The same interpolation was done with the wind data from ERA Interim [7] [30]. The software package of the WAM model is made flexible so the user may choose the composition of the output data. The grid point spacing was 0.08 degrees and WAM was run with a 5-minute integration time step. 151 is the number of zonal grid points, and 226 is the number of the meridional grid points. The two-dimension spectral boundaries were fixed with 25, logarithmically spaced, frequencies ranging from 0.042 Hz to 0.42 Hz, and with 24, (15 degrees) direction bins (resolution).

The model output was set up for every 3 hours and the time used on the model was UTC (coordinated universal time). The model was run month by month with a cold start [1] only for the first (January) month. The subsequent model runs were warm starts, which means that they just continue from the end state of the previous run.

[1] A cold start means that the model starts with a parametric spectrum corresponding to low winds.

3.4 Satellite wave measurements

Surface wave height can be estimated empirically using microwave sensors transmitting electromagnetic energy (EM). Information about wave conditions at the Sea surface can be obtained by analyzing the reflected signal and comparing the parameters from waveform with the theoretical parameter curve. The basic graphical outlines of reflected signal over the ocean shown in Figure 3.3.

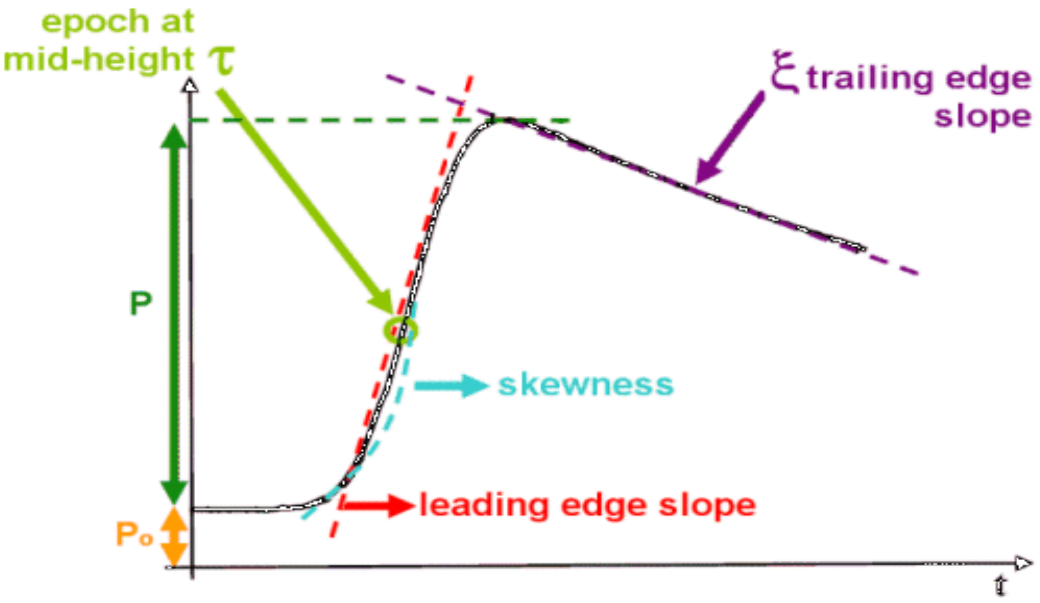

FIGURE 3.3: Graphical outline of reflected signal over the ocean [28].

From this figure six parameter an be obtained, epoch at mid-height give you the delay reflected back of the radar pulses, P is the amplitude of the signal, P_0 is thermal noise, leading edge slope is related to the significant wave heights, skewness is the leading edge curvature, and trailing edge slope linked to any deviation from nadir of the radar signal [28].

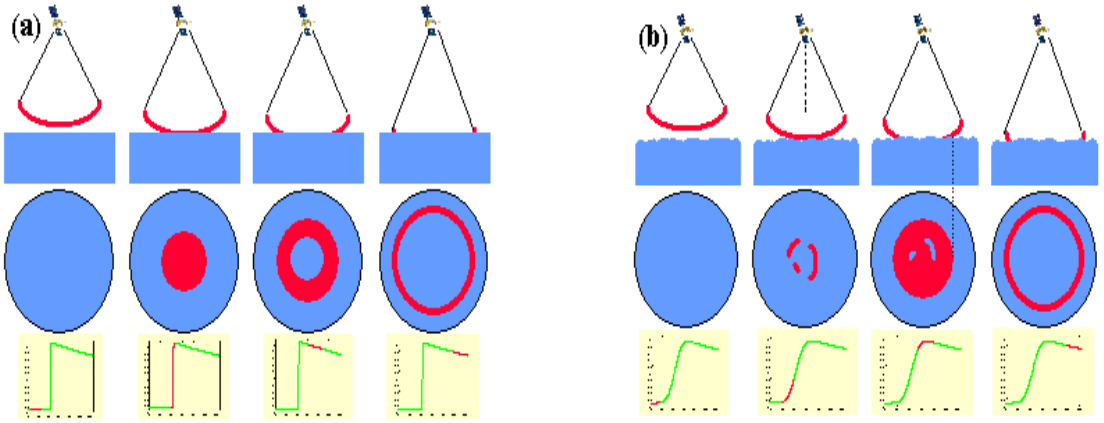

FIGURE 3.4: Scheime of haw the alimeter radar receives the reflected signal from (a) flat sea surface and (rough) sea surface [28].

Figure 3.4 shows how is the altimeter radar receives the reflected signal, the amplitude of the reflected signal from flat sea surface, Figure 3.4 (a), start to increase sharply when the signal touch the surface, see the leading edge. In rough sea, Figure 3.4 (b), the signal reflect from one crest and then from other series of crests which make the amplitude of reflected wave increase progressively [28].

3.5 Data description

3.5.1 ERA-40

The ERA-40 data base is a global atmospheric reanalysis that contains atmospheric and wave parameters for the period September 1957 to August 2002 [27]. The objective of the ERA-40 project was to create high quality reanalysis for the past four decades; *for more details see* [30].

In this study the ERA-40 data was used to estimate out the maximum wind speed in the Red Sea from 1957 to 2002.

3.5.2 ERA interim reanalysis

ERA-Interim is a reanalysis of the global atmosphere covering the data-rich period since 1989, and continuing in real time. ERA-I is an "interim" reanalysis of the period 1989-present in preparation for the next-generation extended reanalysis to replace ERA-40. The ERA-Interim project was initiated in 2006 to provide a bridge between ECMWF′s previous reanalysis, ERA-40 (1957-2002), and the next-generation extended reanalysis envisaged at ECMWF; *for more information see* [7].
In this study a hindcast over a full 1-year period is presented. The significant wave heights hindcast for 2007 by the WAM model as implemented at the European Center for Medium Range Weather Forecasts was compared with previous study and show good agreement in general. The wind applied to force WAM was extracted from the ECMWF ERA interim reanalysis.

3.5.3 Altimeter data

The altimeter data have been used extensively by the science community across the globe by providing estimates of sea surface height. The altimeter data from ENVISAT [26] , JASON [16] and GEOSAT-FOLLOW ON (GFO) [1], were compiled and quality checked by IFREMER, the French marine research institute, *for more details see* [24].

Chapter 4

Result

In this chapter we will illustrate the wave conditions in the Red Sea using a one-year WAM integration. We also study the maximum expected wave height through test cases with constant wind.

4.1 One year WAM integration

In this section we will show the result of the integration for one year, 2007. Then we can extract information about the wave height, wind direction and wind speed in the Red Sea.

4.1.1 Wave height and wind direction in the Red Sea

The Red Sea has complicated wind forcing with surface winds that can reach speeds of 12 ms^{-1}. In this one-year integration we will focus on the seasonal circulation patterns. The direction of the surface winds is orographically steered more or less along the axis of the Sea and that is due to the existence of high mountain ranges along the African and Asian coasts. Figure 4.1 illustrates the wave height simulated for January from WAM. Two wind regimes are present, one in the northern part of the Red Sea and one in the southern part. Maximum wave height 1.8 m is located between 19.5^{o}N and 24^{o}N.
Also the minimum wave height 0.2 m found in Gulf of Aqaba, Gulf of Suez and Bab Al Mandab Strait. The wind during this month, Figure 4.2, blows along the axis of the Red Sea from the north-west from 30^{o}N to 18^{o}N

But from latitude 18^{o}N and going southwards winds start to change their direction until it reverses in Bab Al Mandab. In this month the mean wind speed

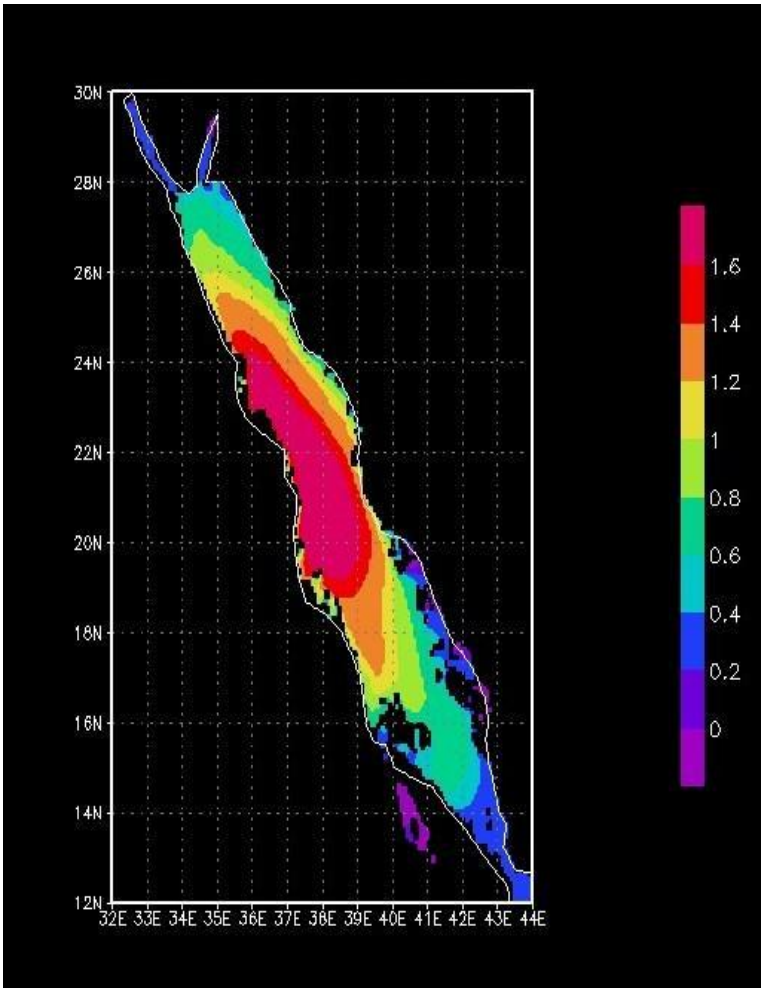

FIGURE 4.1: Wave height in Red Sea from WAM model, The result represent the end state after a one-month simulation, January 2007.

is 10 ms^{-1}. When we try to compare these two figures (wave height and wind speed) we see in Gulf of Suez where the fetch is short, we record the minimum wave height and waves increase their height with decreasing latitude, reach maximum and start to decrease their height with changing the wind direction in Bab Al Mandab.

On other hand if we take a look at the wave height for July (summer), see Figure 4.3, we see the maximum waves height [1.4 m] located in two places, the northern part of the Sudanese coast and the southern part of Sudanese coast. This month represents summer time in Red Sea, and here the minimum wave height found is 0.3 m near Sudan coast and also Gulf of Suez, Gulf of Aqaba as well as near Bab Al Mandab .

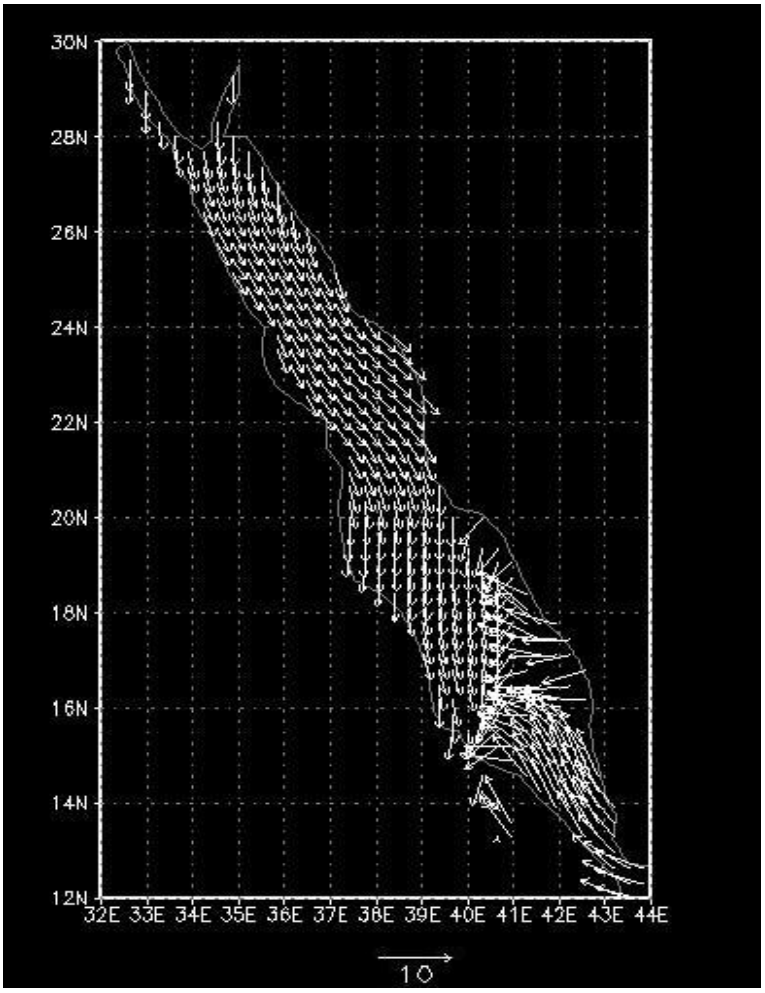

FIGURE 4.2: January 2007, the winds at 21h 31 January 2007.

This feature can be more understandable if we take a look on wind direction for July 2007, see Figure 4.4.

This figure shows complicated feature of wind direction, we see here winds coming from north west, traveling along the axis of the Red Sea. As we know, in summer time there is no strong wind that could create these maxima we seen in Figure 4.3. South east winds pass Bab Al Mandab and traveling forward, these two maxima of wave heights appear in the same Figure 4.3 [1] it is swell heights.

[1] In land wave appears in WAM result in 14^oN 40.5^oE it seem to be an error in topography WAM file. There is no river in these area.

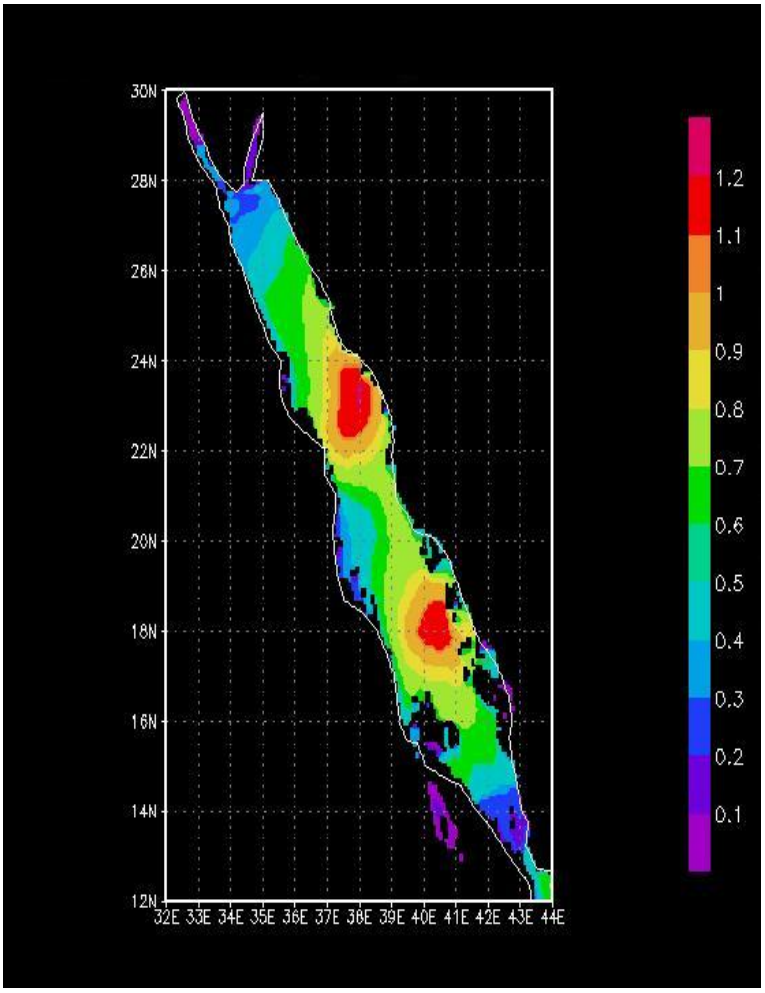

FIGURE 4.3: Wave height in Red Sea from WAM model, The result represent the end state after a one-month simulation, July 2007.

It appears that the wind direction in the Red Sea has three regions, northern region is between 30^oN and 20^oN, southern region is between 16^oN and 12^oN and the intermediate region where is between 20^oN and 16^oN. By comparing Figure 4.4 with Figure 1.2 (a) we see that north west wind blow along the axis of the Red Sea in the two figures, at the strait of Bab Al Mandab some winds flow into the Red Sea from Arabian Sea.

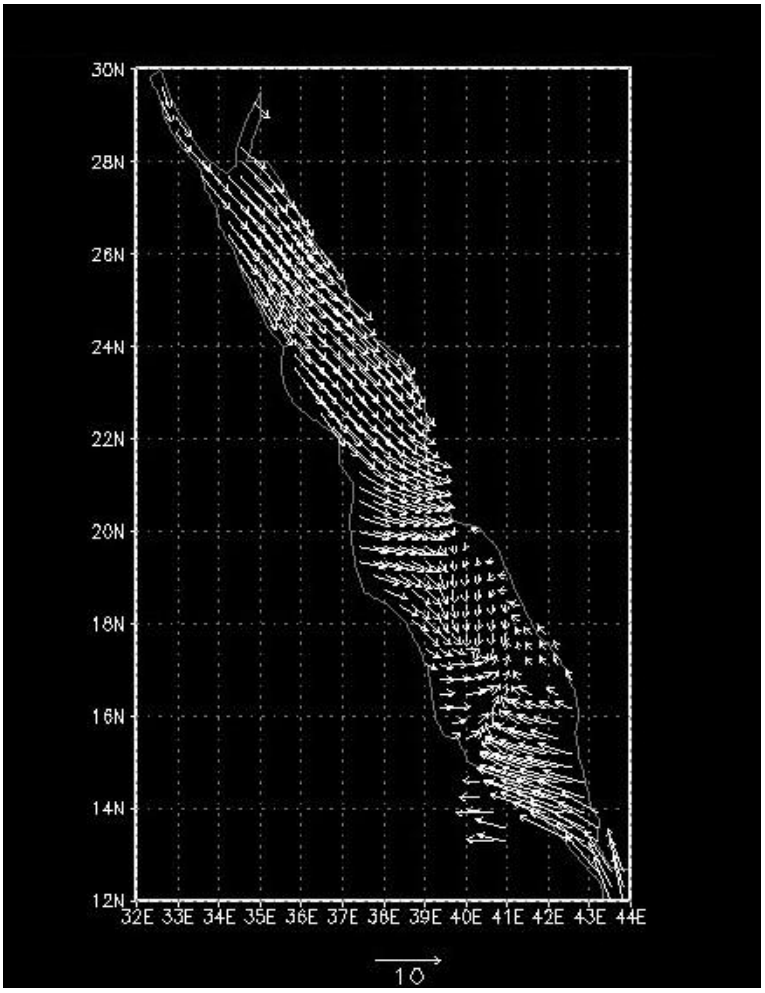

FIGURE 4.4: July 2007, the winds at 21h 31 July 2007.

4.1.2 Extraction of information for fishing ground areas in Red Sea from WAM output

Four fishing grounds have been studied in this thesis. We chose the areas Port Sudan, Sawakin, Mohamed Qol and one area in the middle of the Red Sea. See Figure 4.5.

For these areas we will take only one month for every area and extract information about the maximum wave height, wind speed and wind direction.

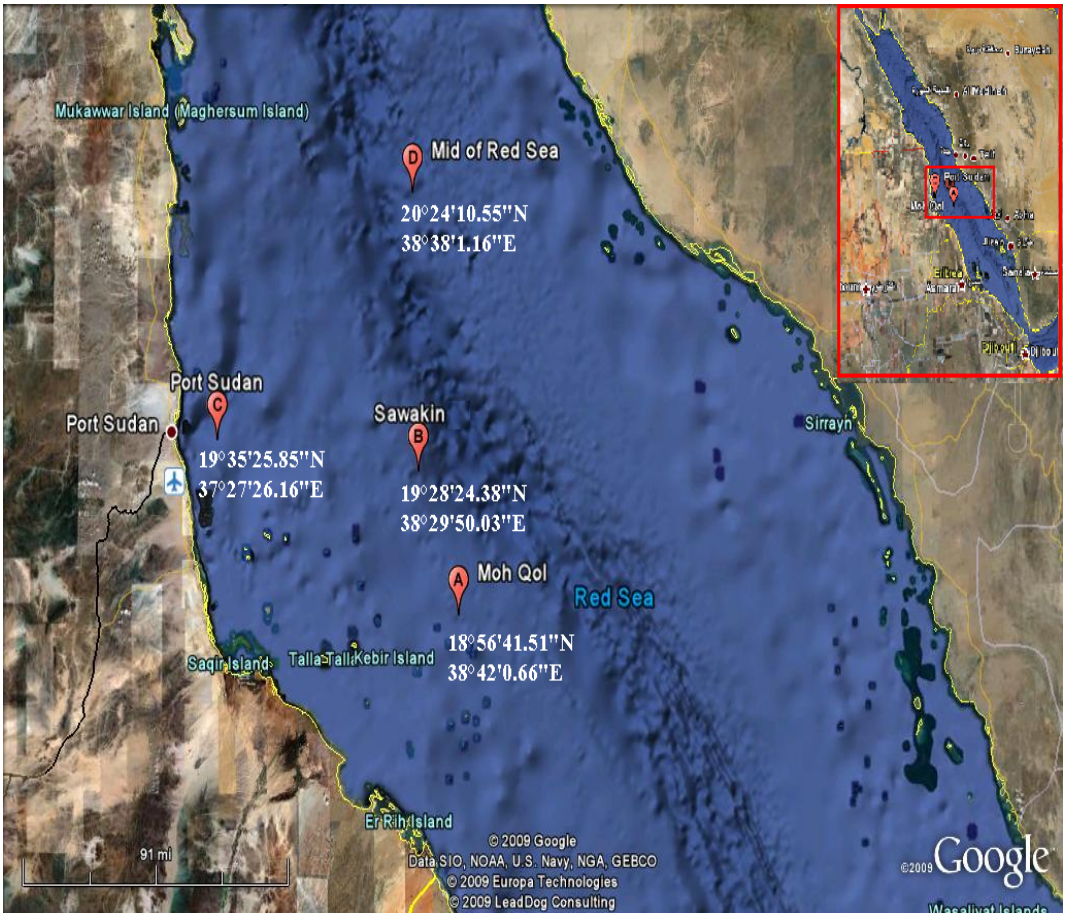

FIGURE 4.5: Most used fishing ground areas in Red Sea (Google earth).

4.1.2.1 Port Sudan

Figure 4.6 shows a time series of wave height and wind speed for Port Sudan [19^{o}35$'$N 37^{o}27$'$E] fishing area during January 2007. In this figure also we see very high correlation between wave height and wind speed. The maximum wave recorded in 05.01.2007 is about 2 m and corresponding to maximum speed which is about 12 ms^{-1}.

The minimum wave height is about 0.2 m, recorded 27.02.2007 and it is corresponding to minimum wind speed in the same date, about 2.4 ms^{-1}. In Port Sudan winds in this month blow along the axis from north to south as we show in Figure 4.2. The wind statistic for January is found in Figure 4.7.

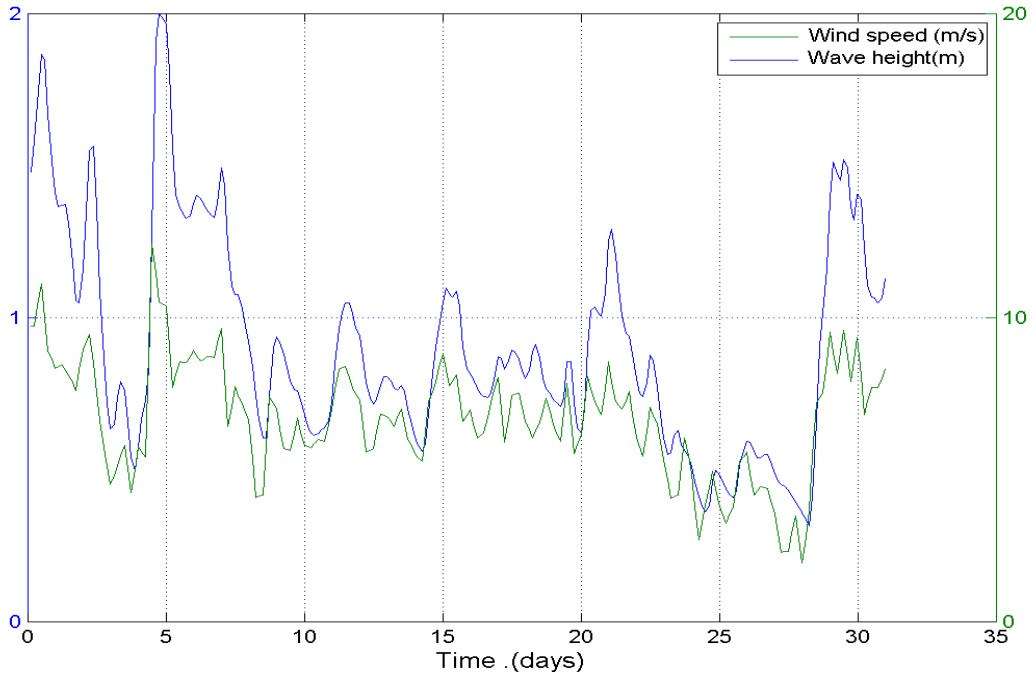

FIGURE 4.6: Time series of wind speed and wave height at Port Sudan , January 2007.

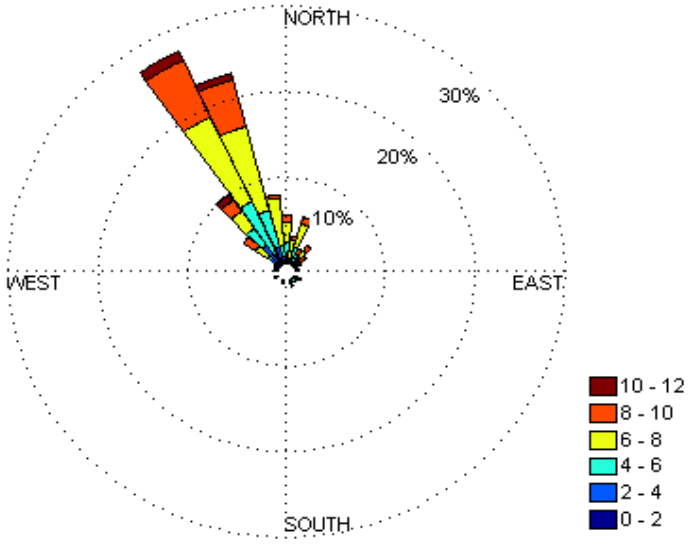

FIGURE 4.7: Wind rose plot shows wind direction at Port Sudan during January 2007.

Shown in Figure 4.7 is the January wind rose for Port Sudan 2007. This rose shows that the winds at Port Sudan fishing area in January blow from the north-west much of the time. In fact the three spikes around the north west direction comprise about 60% of all 3 hour wind directions. Maximum wave height is about 2 m recorded at the end of day 04.01.2007 corresponding with the maximum wind speed about 11 ms^{-1} recorded earlier at the beginning of 04.01.2007. Due to the short distance between Port Sudan and Suakin the time series of wind speed and wave height and wind rose plot for wind direction at Suakin looks more or less same as in Port Sudan. The maximum wave height in Suakin is 2 m and maximum wind speed is 12 ms^{-1}; for more details see appendix D.1 and D.2.

4.1.2.2 Mohamed Qol

In Figure 4.8 we present time series for January 2007 of wave height and wind speed in Mohamed Qol [$18^o56'$N $38^o42'$E]. More or less the same wave height maxima and the same wind speed are seen as in Port Sudan. Figure 4.9 illustrates the wind direction for Moh. Qol, showing more northerly winds than recorded in Port Sudan.

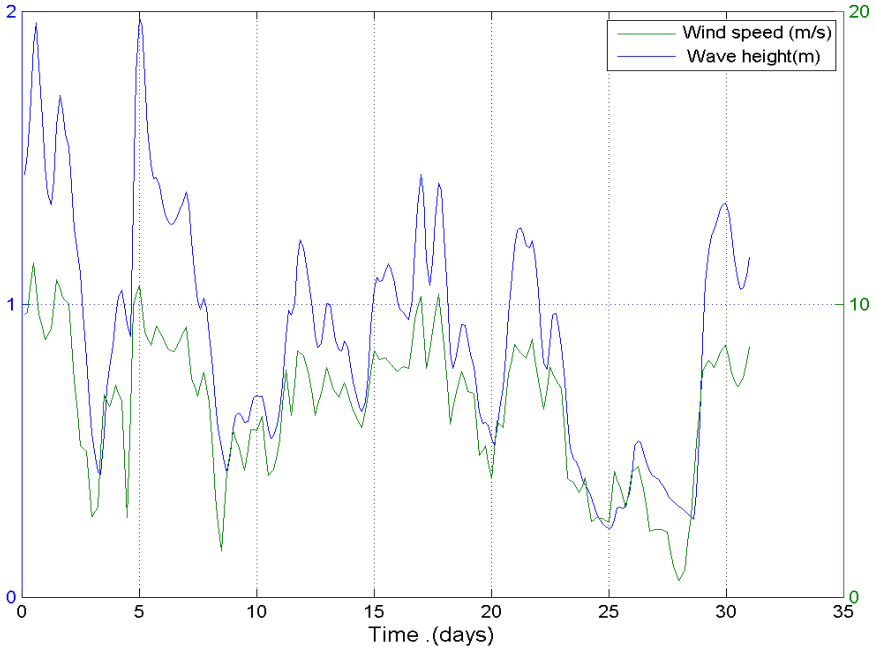

FIGURE 4.8: Time series of wind speed and wave height at Moh Qol, January 2007.

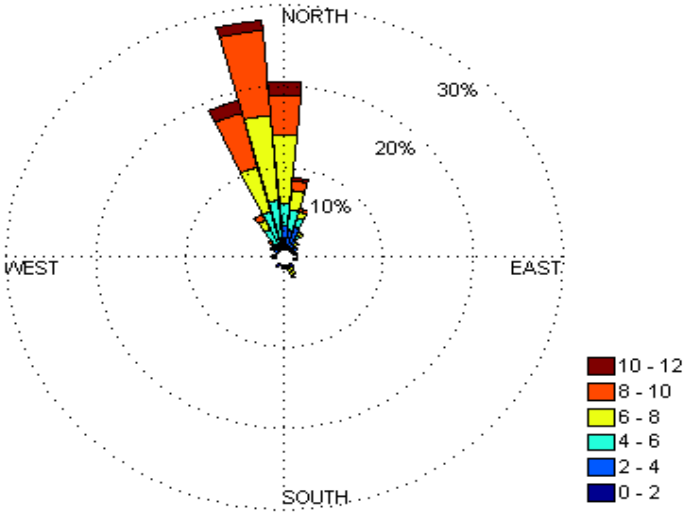

FIGURE 4.9: Wind rose plot shows wind direction at Moh. Qol during, January 2007.

4.1.2.3 Middle of the Red Sea

The last, but not the least fishing ground we present is located in the middle of the Red Sea [$20^o24'$N $38^o38'$E]. Figure 4.10 presents time series of wind speed and wave height during January 2007. In this location the maximum wave height is about 2.1 m and maximum wind speed is about 12.5 ms^{-1} between 04.05.2010 and 05.01.2007. As this point is located in the middle of the Red Sea we see a lot of variations which could be a result of interference of wind sea and swell.

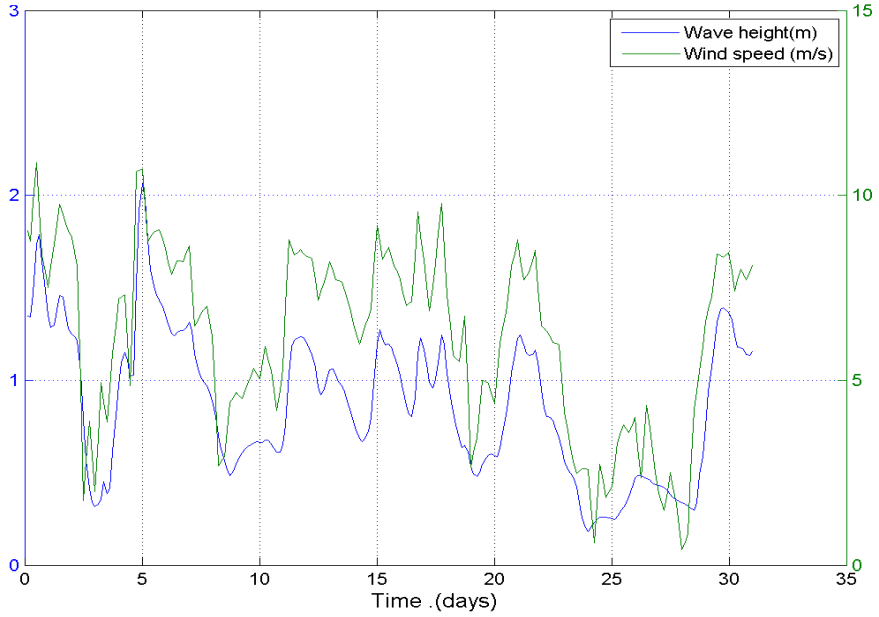

FIGURE 4.10: Time series of wind speed and wave height at Middle of the Red Sea , January 2007.

Figure 4.11 shows more or less the same directional features (north westerly wind) and that is a result of the monsoon wind during this month. Also a few bars show that there are some winds coming from the north east.

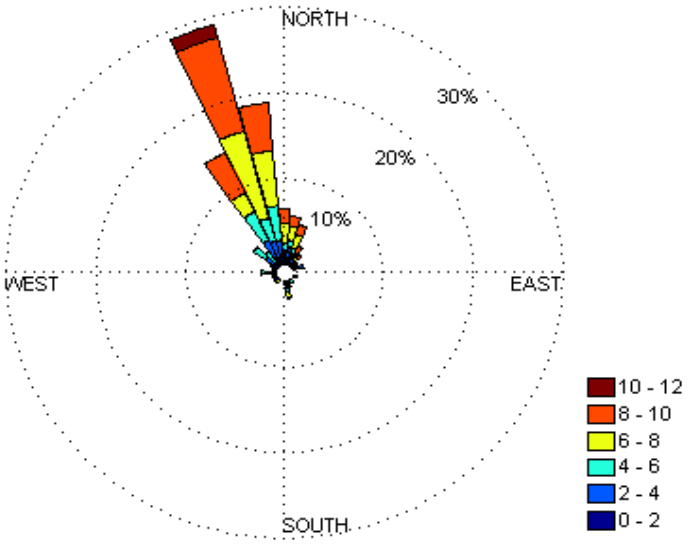

FIGURE 4.11: Wind rose plot shows wind direction at Middle of the Red Sea during January 2007.

In Figure 4.12 histograms of significant wave height are plotted for (a) Port Sudan and (b) Moh. Qol. In Port Sudan the most frequent height during 2007 was between 0.6 and 1 m. But during the same year we found also wave heights reaching 2 m. In Moh. Qol the most frequent height recorded was between 0.5 and 1 m and also there, significant wave heights more than 2 m showing in a few cases during this year, see Figure 4.12 (b).

As we mentioned earlier, the WAM model was run every month during year 2007, and that means we have 12 WAM monthly grid outputs. One of the important parameter we studied is swell height. It is very interesting to see how large the swell height can be to see if it could be dangerous for fishermen or not.

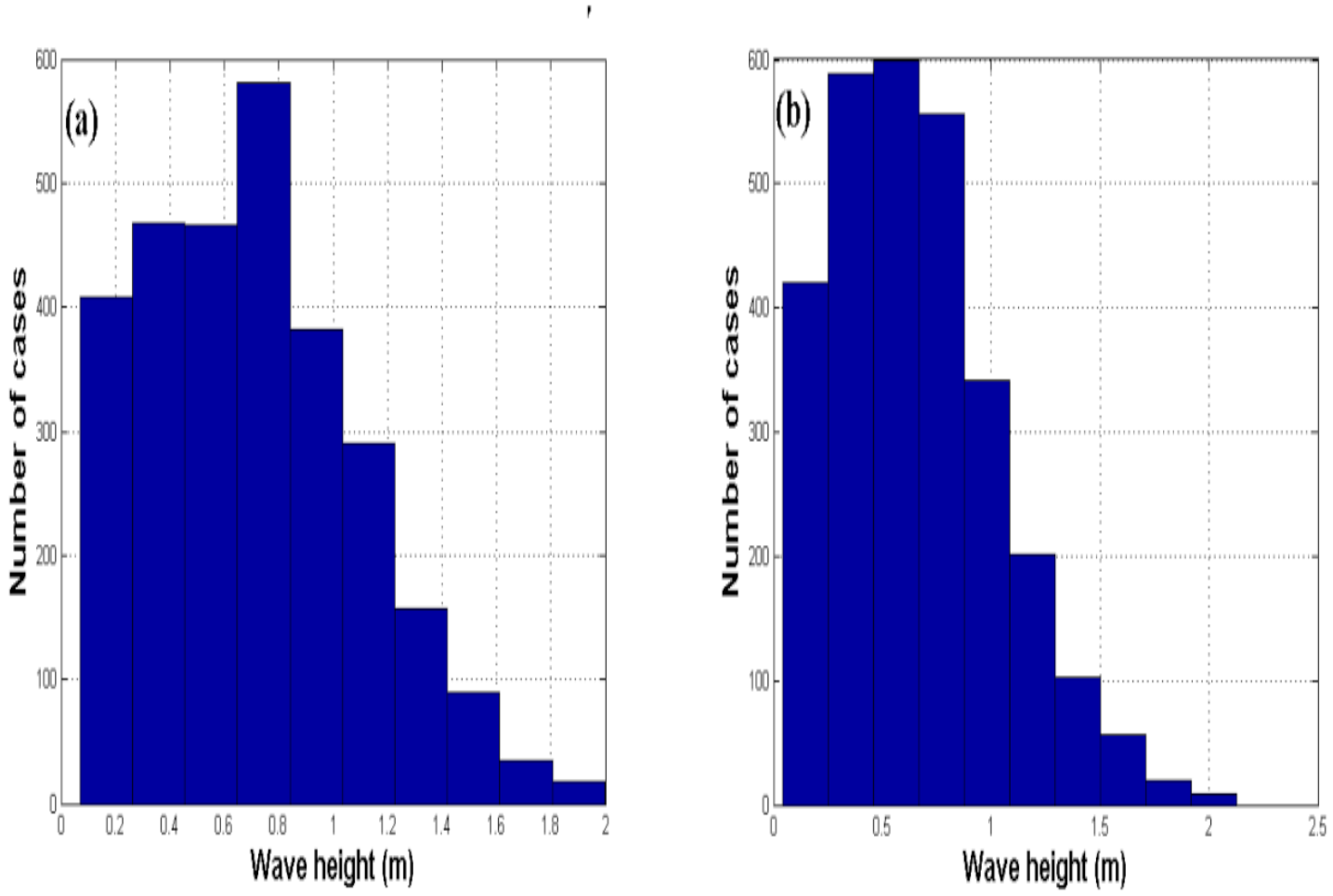

FIGURE 4.12: Histogram of significant wave height in the Red Sea for the whole 2007, (a) Port Sudan and (b) Moh. Qol.

Figure 4.13 illustrates a histogram of swell height for two locations in the Red Sea during 2007. Port Sudan Figure 4.13 (a) seems to be more safe for the fishermen than Moh. Qol Figure 4.13 (b), the dominant swell height in Port Sudan was 0.4 m and in a few cases we modeled heights of 1 m and more. This can be dangerous.

In Moh. Qol swell height can reach 1 m and more in a few cases, which could be dangerous for small fishing boats.

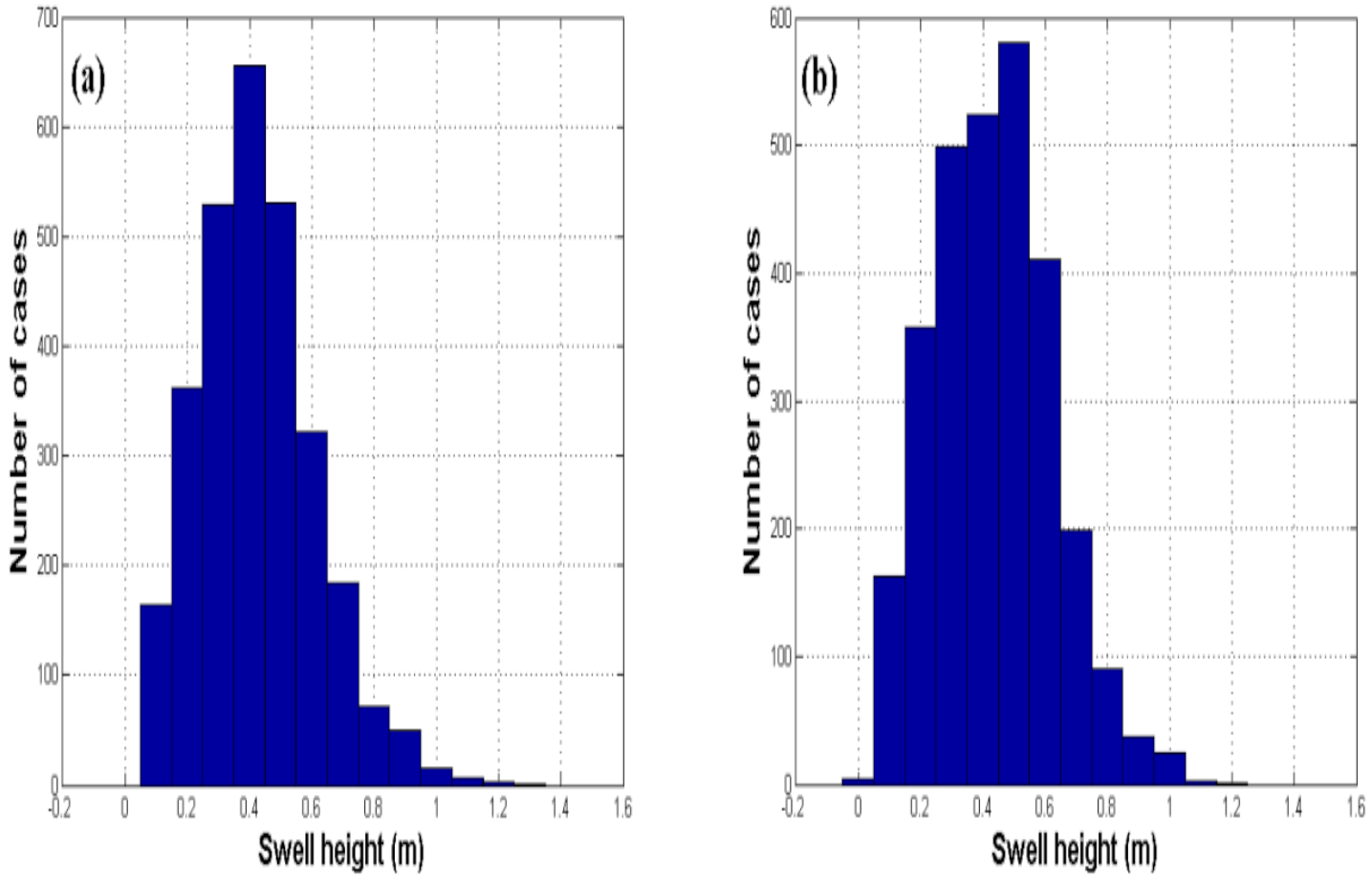

FIGURE 4.13: Histogram of swell height in the Red Sea for the whole 2007, (a) Port Sudan and (b) Moh. Qol.

A histogram of wind speed in Port Sudan and Moh. Qol also was plotted and we found that the wind speed varies between 0 and 13 ms^{-1}, for more details see appendix D.3.

Figure 4.14 also shows a histogram plot of wind speed in (a) Suakin and (b) Middle of the Red Sea. In Suakin Figure 4.14 (a), we see that the speed varies between 0 and 13 ms^{-1} and the most dominant speed was between 6 and 8 ms^{-1}. In the middle of the Red Sea Figure 4.14 (b), we see the same range of speed between 0 and 13 ms^{-1}, but low wind speeds are more frequent.

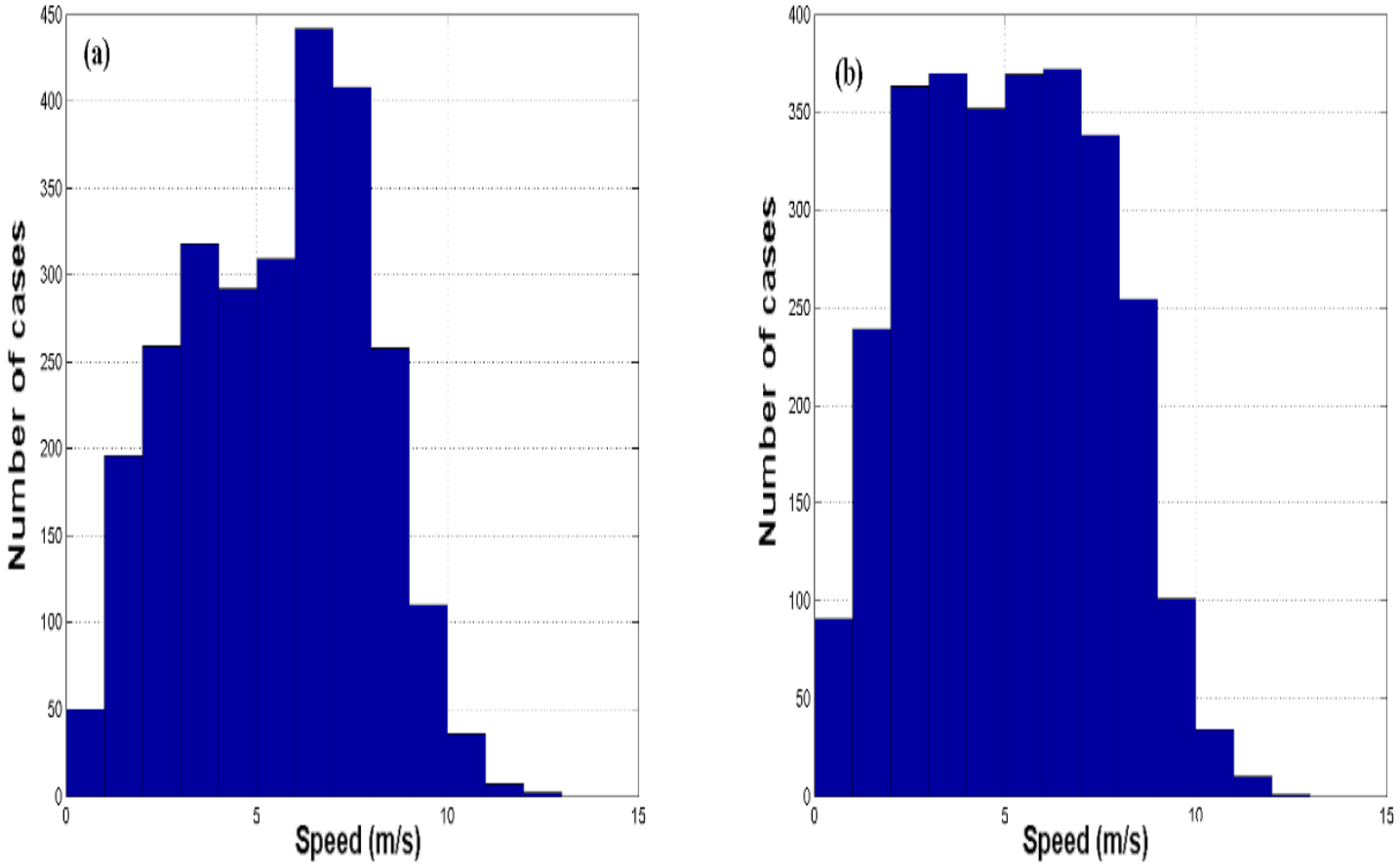

FIGURE 4.14: Histogram of wind speed in the Red Sea for the whole 2007, (a) Suakin and (b) Middle of the Red Sea.

A histograms of significant wave heights for Suakin and Middle of the Red Sea described in appendix D.4.

An interesting result is to see how often we can get waves higher than 1 m or 2 m at the four fishing grounds.

4.1.3 Time fraction of high waves

The sum of all columns in the histogram in above plots is equal to 100 % of cases and the sum of all columns belonging to wave heights (N) divided by the total sum (tot) will give us the time fraction. So we can write down the equation as below:

$$Time\ fraction = \left(\frac{N}{tot}\right) * 100\% \tag{4.1}$$

Where N, is the number of cases of the wave height, and [tot] is the total number of cases.

To see the percent of cases in all fishing grounds of getting significant wave heights more than 1 m and more than 2 m, see Table 4.1.

TABLE 4.1: **Percent of time fraction of high waves in all fishing grounds**.

Location	Time fraction of high waves	
	More than 1 m	More than 2 m
Port Sudan	22.5%	0.00%
Moh. Qol	17.6%	0.10%
Suakin	22.6%	0.00%
Middle of the Red Sea	20.7%	0.24%

In Port Sudan and for wave height more than 1 m the time fraction is 22.5%, and that means in 22.5 % of the cases in Port Sudan we can get significant wave heights more than 1 m; see Figure 4.12 (a). This means that we can get maximum wave hieghts over 2 m during a 6h-period in 22.5 % of the time, [21]. No cases in Port Sudan can get significant wave heights more than 2 m.

In Moh. Qol, result shows that Moh. Qol is more safe for the fishermen than Port Sudan, because high waves are less frequent. For wave height more than 2 m time fraction in Moh. Qol is 0.10%, this means that there will be maximum wave heights over 4 m about once every third year at Moh. Qol.

In Suakin the percent approximately similar as in Port Sudan. Suakin is the one of the active fishing ground and most of fishermen using small boats near shore which could be unsafe after few hours. Middle of the Red Sea is located in the middle of the Red Sea [$20^o24'$N $38^o38'$E]. This fraction percent put the middle of the Red Sea on a list of safe ground , because this point in center of the Red Sea which small boat can not reach , while big ships can sail without facing any trouble.

The fraction of high waves more than 2 m in the Middle of the Red Sea is also very small and will not make any trouble for the big ships.

4.2 Constant wind experiment

The aim of constructing this experiment is to see what the maximum wave height we can get in Red Sea is and where. To run the WAM model with constant wind, we had to adjust the model code according to specified wind speed and direction.
Secondly we must determine the maximum wind speed in the Red Sea. A subset of the ERA-40 data (1960-2001) was used to find the maximum wind speed in the Red Sea. Two places were selected and wind rose of wind speed and direction in Red Sea from 1960 to 2001 were plotted, see Figure 4.15 at 18^oN 40^oE and Figure 4.16 at 15^oN 42^oE. These figures illustrates the 42 years for the selected two locations. but we can see that the maximum wind speed is about 12 ms^{-1}.

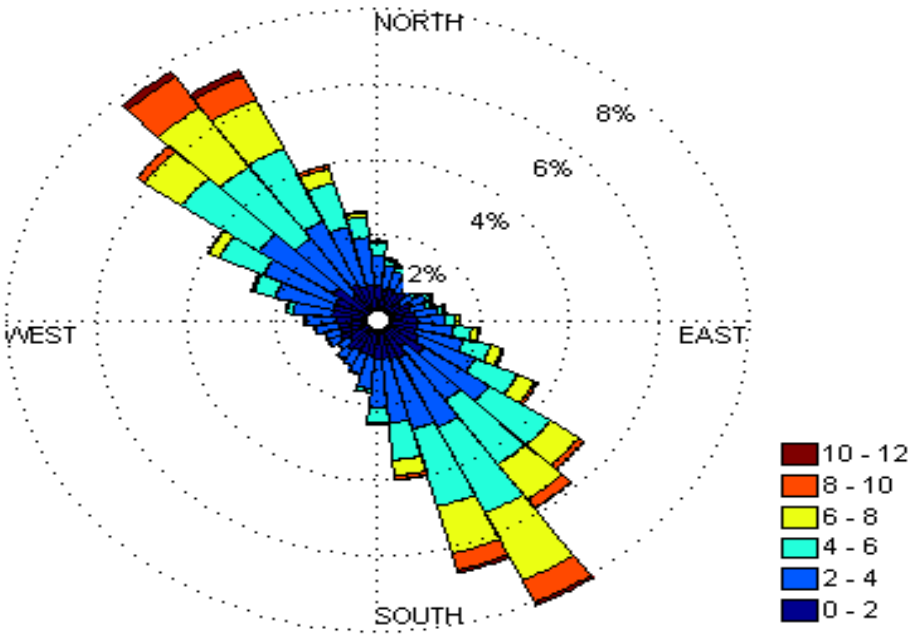

FIGURE 4.15: Wind rose plot of wind speed and direction at 18^{o}N 40^{o}E in the Red Sea from 1960 to 2001.

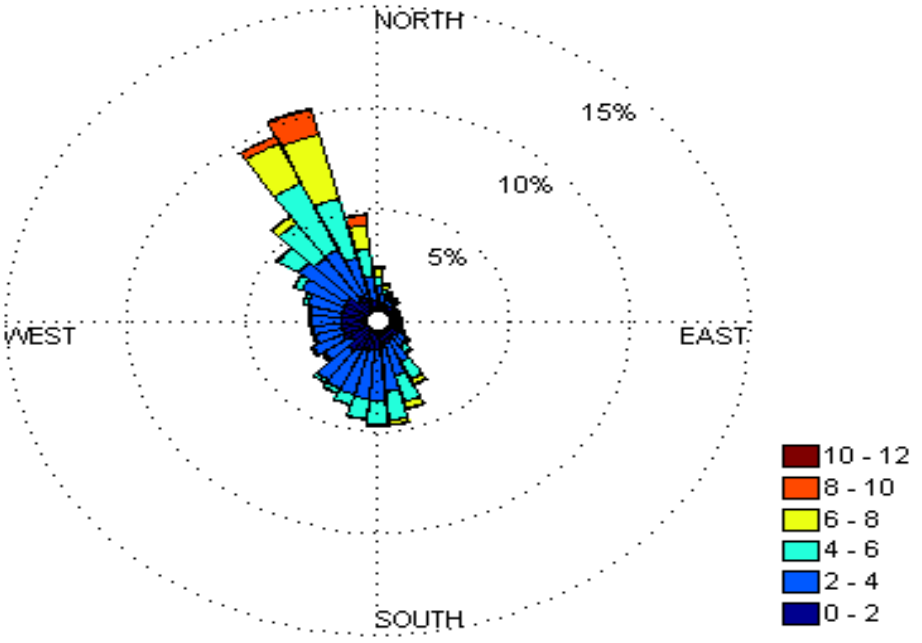

FIGURE 4.16: Wind rose plot of wind speed and direction at 15^{o}N 42^{o}E in the Red Sea from 1960 to 2001.

As we mentioned above, some changes were made in one of the WAM programs to set it to be flexible to choosing the wind direction and speed.
WAM was run for 3 days with constant wind 12 ms^{-1} and we chose to run WAM with wind along the Red Sea, first from north to south. Figure 4.17 shows the wave height field in this case.

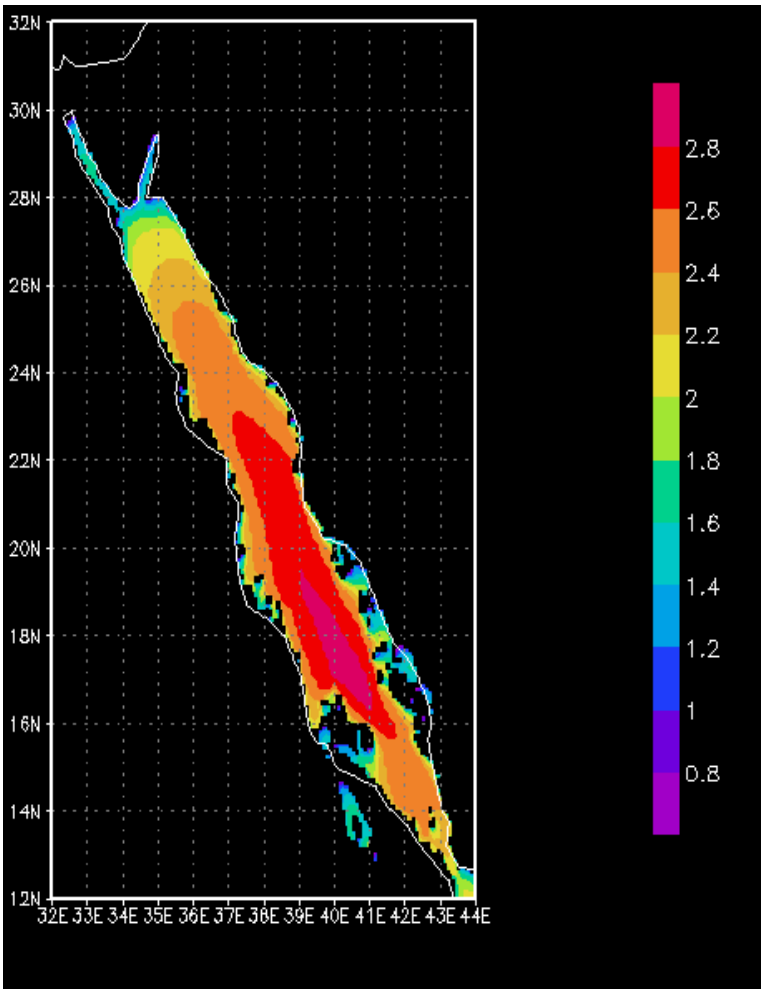

FIGURE 4.17: Wave height in the Red Sea after three days of constant wind along the Red Sea axis from north to south.

According to the experiment we made, the fetch is shortest in the north, so we record minimum wave height their. Further south the fetch is unlimited and the interference of swell and wind sea results in higher waves. Wind sea has a quit broad directional spectrum. The narrowing coastline will therefore lead to some loss of energy .

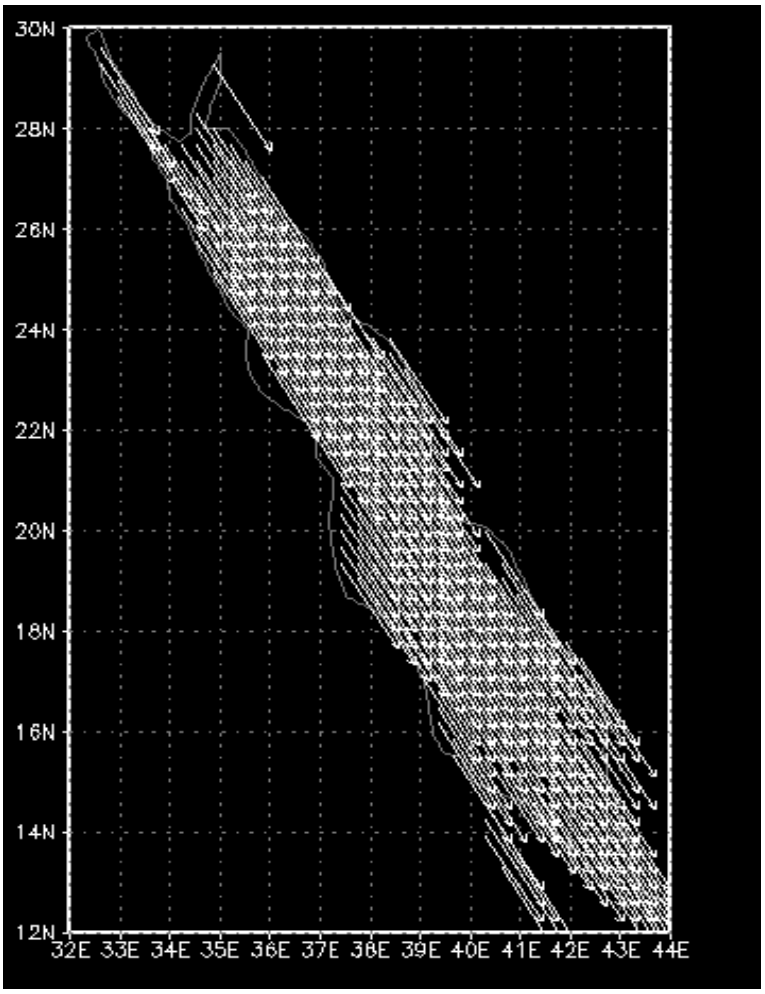

FIGURE 4.18: Wind direction in the Red Sea from WAM.

Figure 4.19 confirms that three-day simulations are sufficient to reach fully developed sea. We see that the wave height starts to increase until it reaches the maximum after about 2 days and then remains stable.

The same experiment is done with 12 ms^{-1} wind blowing from south to north, see Figure 4.20. Minimum wave height recorded was 0.8 m and maximum wave

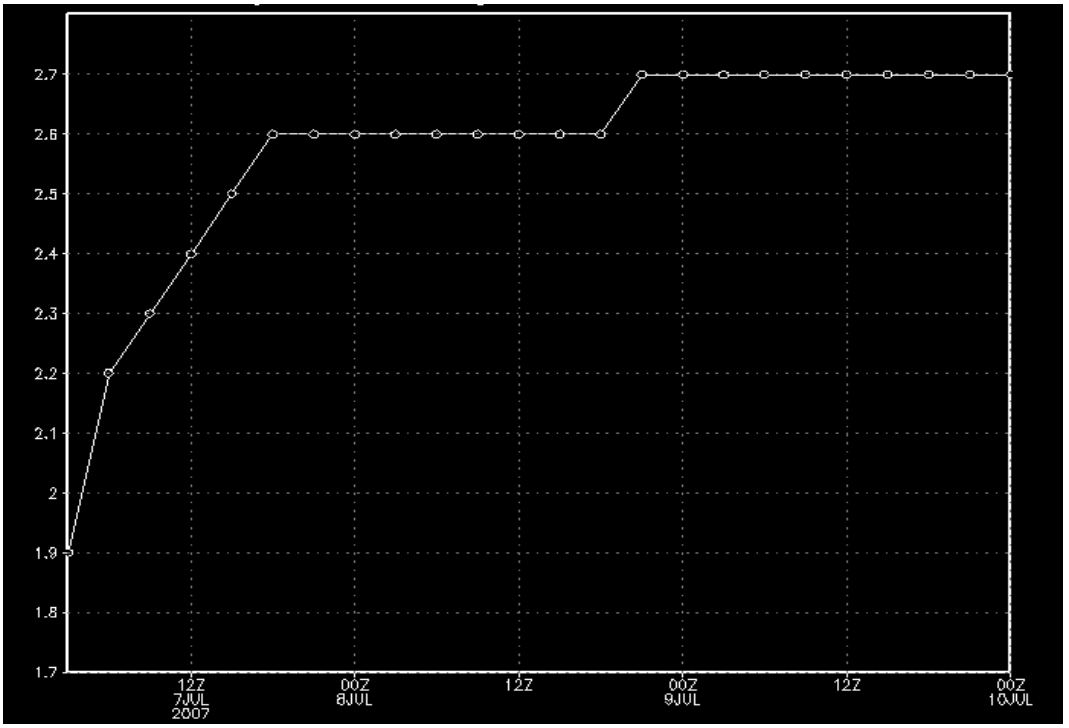

FIGURE 4.19: Wave height time series for the point 23E, 38N in the Red Sea represent three days simulation from constant wind case study.

height recorded was 2.8 m. The general feature that appears here is the increasing wave height with increasing fetch. Also in a few locations near the shore wave heights can reach 2.6 m, which can be dangerous for fishermen near the shore. Figure 4.21 illustrates that winds are blowing from south to north.

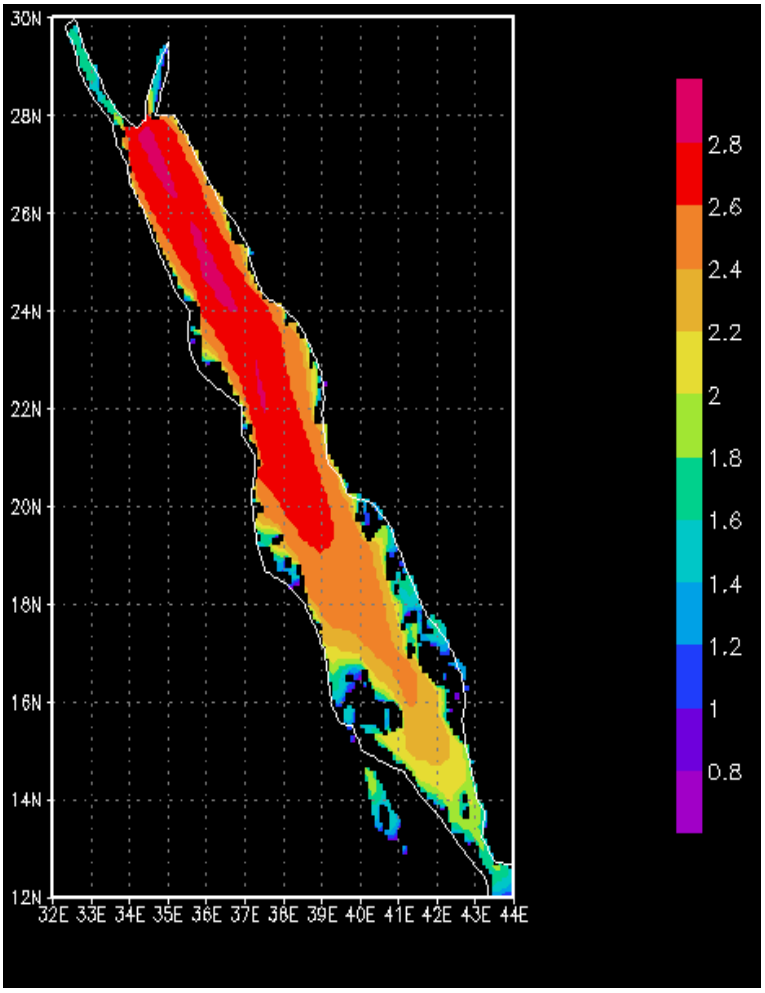

FIGURE 4.20: Wave height in Red Sea as a result of running WAM for three days of constant wind simulation along Red Sea from South to North .

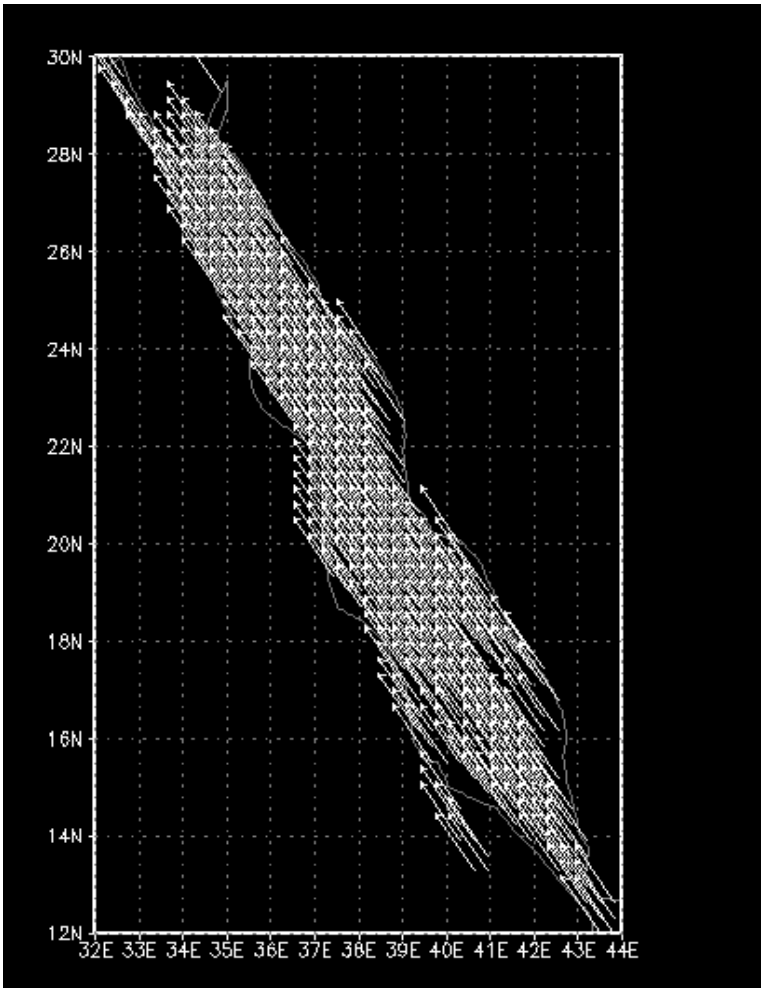

FIGURE 4.21: Wind direction in the Red Sea from WAM.

4.3 Altimeter measurements Vs WAM model data

We have collocated ENVISAT, JASON and GFO, H_s with WAM H_s for 2007. The correlation between measured and modeled significant wave height, H_s, for the Red Sea are illustrated in Figure 4.22.

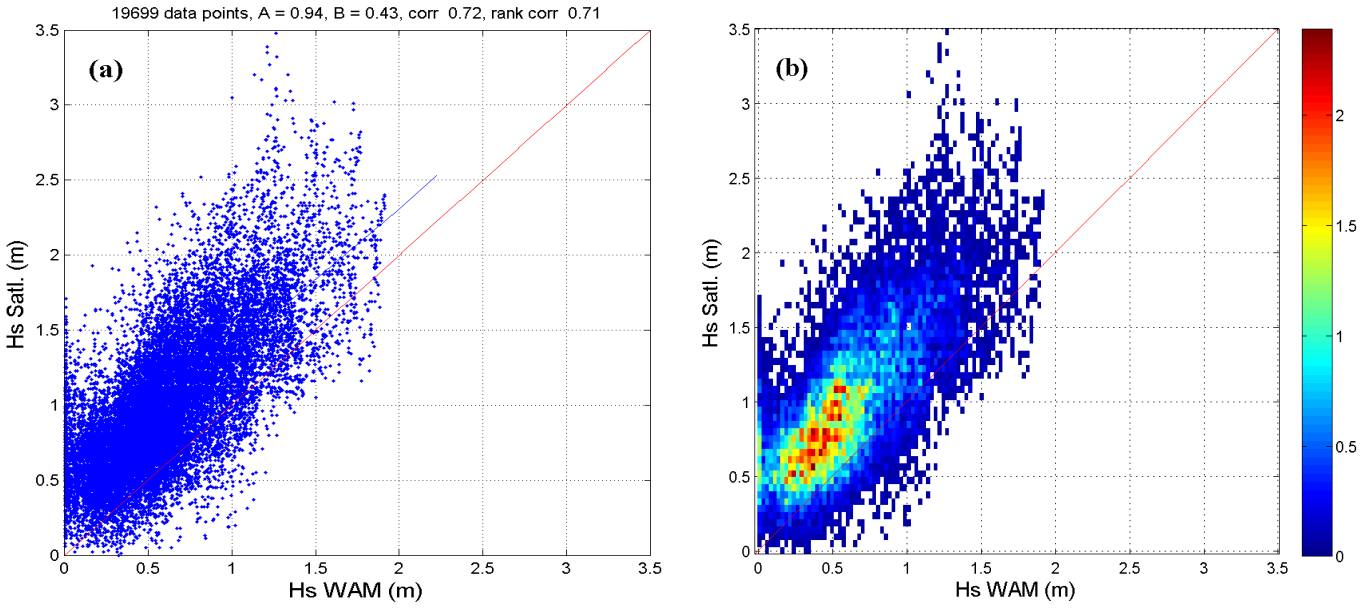

FIGURE 4.22: Correlation between Altimeter and WAM significant wave height data in the Red Sea, (a) linear regression and (b) is probability density.

Figure 4.22 (a) shows the linear correlation between modeled and observed data from satellite. The red line is a 45 degree where modeled is equal to the observed, and the blue line is the regression line between the modeled and satellite data. The blue line is above the red line, which means that WAM is underestimating. From the same figure we see also there is moderate correlation coefficient (0.72) between satellite and WAM wave height data. For example, the highest wave measured not coincident with the hight wave modeled.

Figure 4.22 (b) presents the density distribution, and we see that there is high density in low heights thus, the bulk of the observations are between 0.5 m and 1.25 m and start to decrease with increasing the significant wave height.

It is interesting to see the spatial distribution of the two data set (altimeter and WAM).

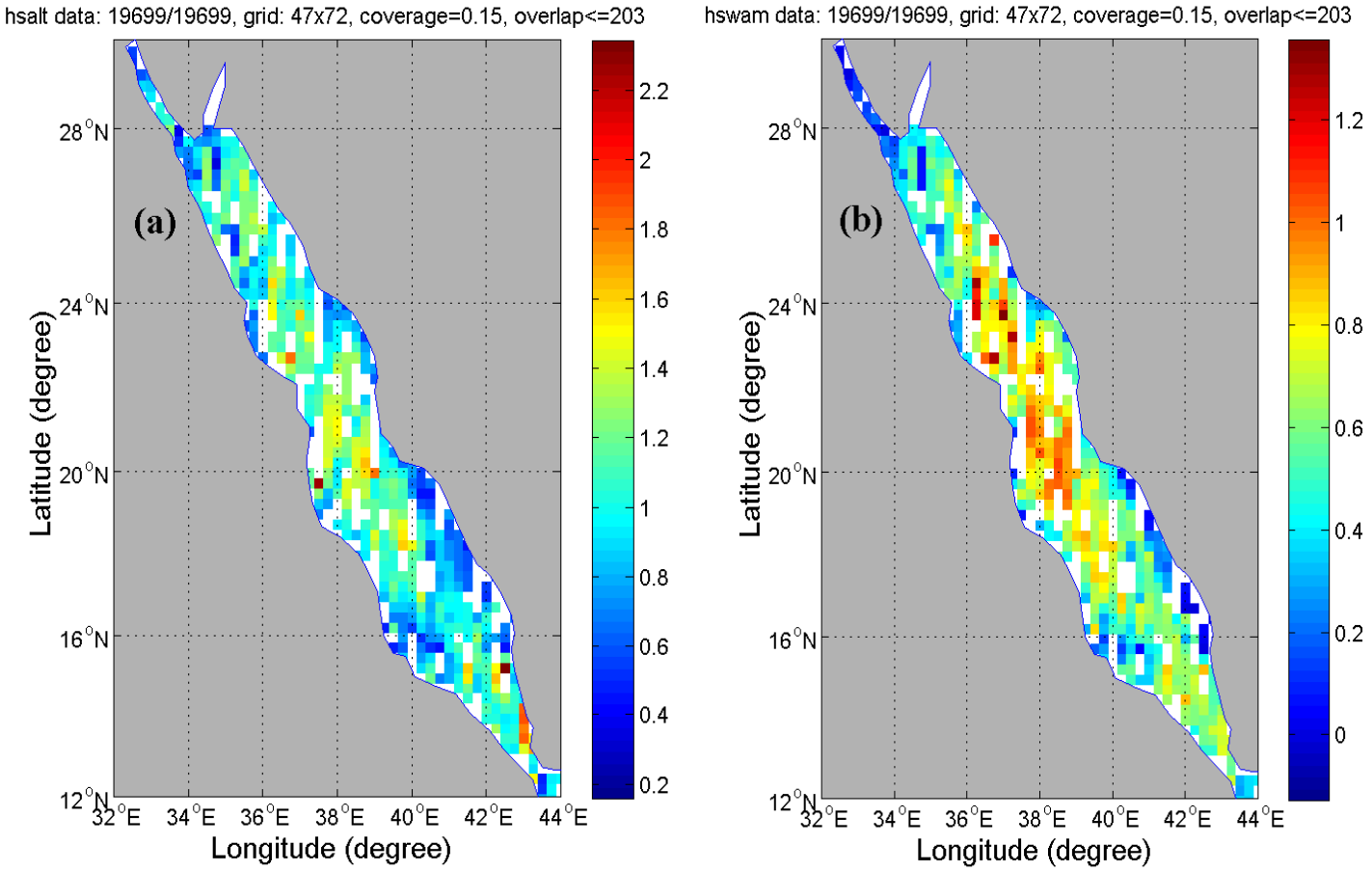

FIGURE 4.23: Spatial distribution of the the two significant wave height data set in the Red Sea whole 2007, (a) altimeter data (b) collocated WAM data; *note the different scale.*

Figure 4.23 illustrates the spatial distribution for the data set for the altimeter data and the collocated WAM data. In Figure 4.23 (a) we see that the maximum wave height is about 2.4 m distributed more or less along the whole axis of the Red Sea in few locations, while in Figure 4.23 (b) the maximum wave height was 1.4 m recorded mostly between 15^oN and 25^oN. The white grid means that there is no data, and that is because the satellite follows fixed repeat orbits, see Figure 4.24 for coverage.

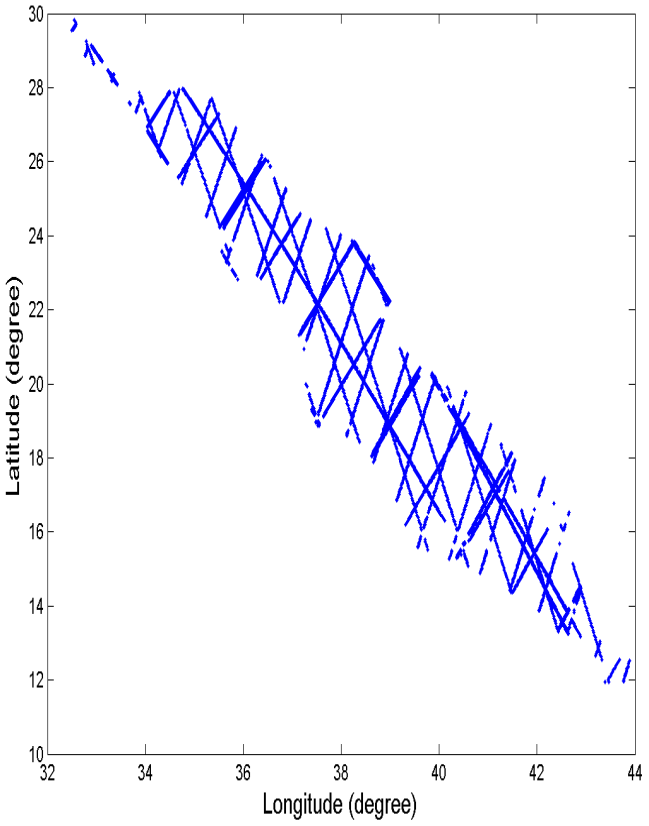

FIGURE 4.24: Altimeter tracks from one year data from ENVISAT, JASON and GFO.

To see where is the big difference between altimeter data set and collocated WAM data, we plot the difference in Figure 4.25.

The color bar is presenting in which places altimeter and WAM data have the same value of wave height and also in which places the wave height is overestimated or underestimated in the Red Sea. The color between red and yellow indicates where the difference between altimeter and WAM data is zero. The wave heights in the Red Sea was overestimated by 0.4 m in few location, while it is underestimated by 1.2 m in few location which appear in dark blue.

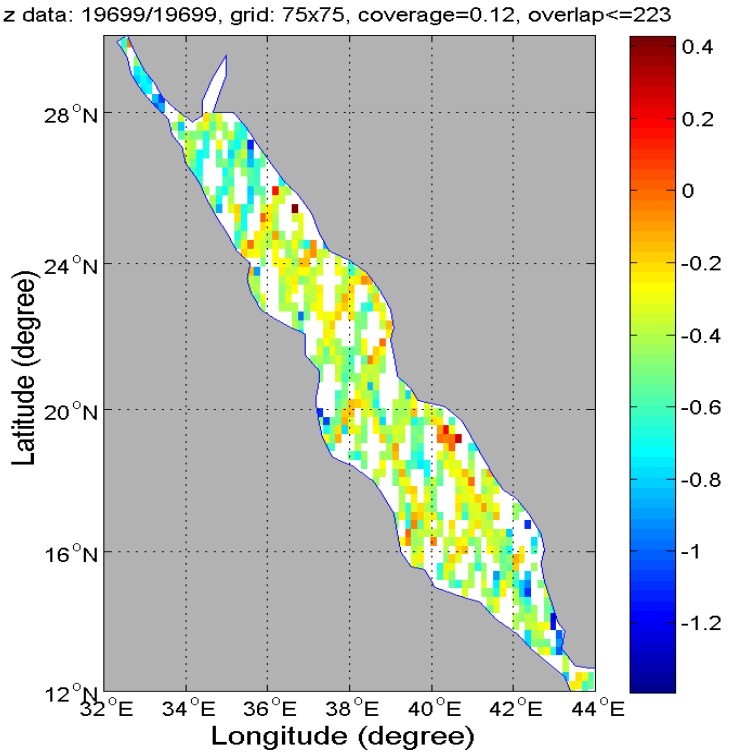

FIGURE 4.25: The difference between altimeter data and collocated WAM data for whole 2007.

Figure 4.26 illustrates a histogram of significant wave height in the Red Sea for the whole 2007. Figure 4.26 (a)shows altimeter wave height and the maximum here was 3.5 m, most dominant wave height is between 0.5 and 1.5 m.

While Figure 4.26 (b) presents WAM wave height, the maxima here is about 2 m, and most dominant wave height recorded was between 0.25 and 1.25 m.

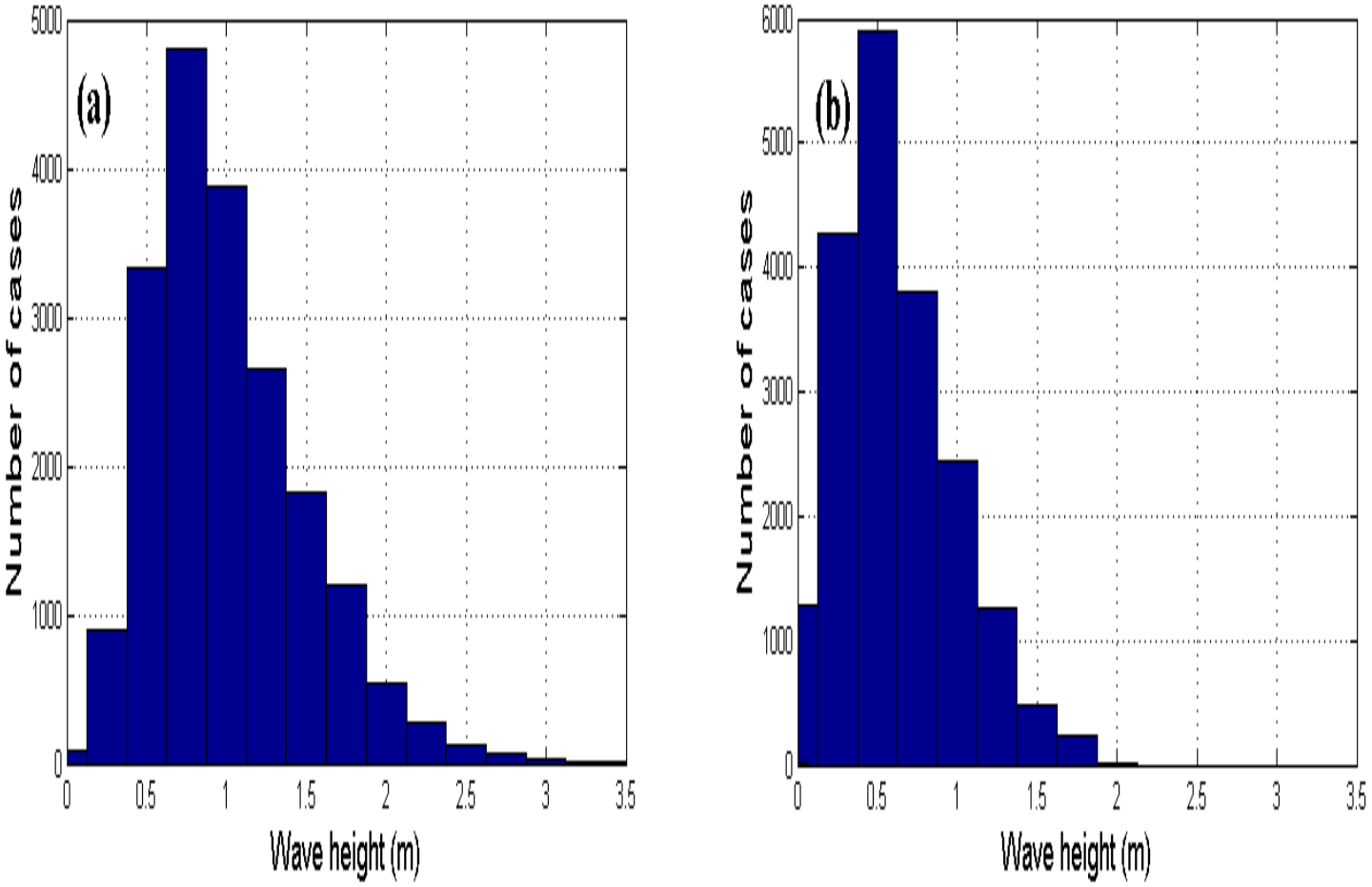

FIGURE 4.26: Histogram of significant wave height in the Red Sea for the whole 2007, (a) altimeter data and (b) collocated WAM data.

Table 4.2 shows the values of the mean, root mean square and the standard deviation. The parameters used for the statistical comparison are all defined in appendix C.2. These parameters are very useful in a validation of a model. Altimeter mean is higher than WAM, consequently, the model underestimates the waves, as already noted earlier. The root mean square shows that the scattering is not that high, this can also seen in Figure 4.22.

TABLE 4.2: **Summary statistics of significant wave height H_s. The RMS is root-mean-square error, Std. dev. is standard deviation**.

Wave height	**Mean**	**RMS**	**Std. dev.**
Altimeter (m)	1.01	1.11	0.48
WAM (m)	0.61	0.72	0.37
Altimeter - WAM	0.39	0.51	0.33

Chapter 5

Discussion

In this thesis significant wave height during varying wind conditions in the Red Sea was studied. High resolution wind fields are important and necessary in wave modeling. The simulated wave conditions depend mainly on the wind forcing. A two day forecast was completed in less than 1 h on a standard Linux workstation. All the months of 2007 were simulated, but two case studies were chosen (winter time - represented here by January - and summer time - represented here by July - in the Red Sea).

Winter monsoon

Figure 4.1 illustrates the wave height at the end of January (winter time) from WAM. Maximum wave height recorded was 2 m located between 19.5^{o}N and 24^{o}N. As mentioned previously in Chapter 1, water circulation in the Red Sea is driven by monsoonal wind patterns. Here winds occur because of the different heating between the land surface and sea in the Indian ocean and Asia. So in the North the monsoon wind is controlled by the eastern Mediterranean weather systems , and that is exactly what appears in Figure 4.2, when we plotted wind vectors for the end of January. Winds in the southern parts of the Red Sea appear in this vector plot to be controlled by the Indian monsoon system. So because of that, winds coming from the North and also monsoon wind coming from the South create a maximum of wave height centered more or less in the middle of the Red Sea and covering the Sudanese coast where most of the fishermen work under more dangerous conditions than elsewhere in the Red Sea.

Generally, when the significant wave height for example H= 2m, the maximum wave height during 6h may be H= 4m [21]. So small fishing vessels used by the fishermen along the Sudanese coast can face real problem to go to the fishing

grounds. Also this simulated wave height was calculated from WAM output every 3 h . If the fishermen sail while there is no high wave it is possible also to to get maximum wave height after 3 or 6 h , because they stay sometimes for some days on the Sea.

Constant wind experiment

The result we got from this experiment gave us good information of what is the maximum wave height we can get and where. ERA40 data was used to figure out what is the maximum wind speed recorded in the Red Sea from 1960 until 2001 to use it to run the WAM model with constant wind . Figure 4.17 clearly shows the effect of fetch as in this experiment we were running WAM with wind forcing from north to south along the Red Sea, it start to generate waves from north of the Red Sea until reach maximum height 3 m. Same thing happens for running the model with constant wind from South to North, and we got the same maximum wave height 3 m. According to Eq.(2.28) fully developed wind sea for a 12 ms^{-1} wind is about 3.5 m.

Now when we know what maximum wave height we can get for a wind speed equal to 12 ms^{-1}, we can make hindcast and forecast also by using this information. The ratio between the maximum wave height from the one year simulation and the constant wind experiment is equal to :

$$\textbf{Ratio = 2 m / 3 m = 0.67}$$

WAM was run every month and we got 12 WAM monthly outputs for the whole year. All monthly files were collected in one file representing the whole 2007 time series, a histogram of wind speed in Figure D.3 shows that speed can reach 13 ms^{-1} in a few cases in Port Sudan and 12 ms^{-1} in Moh. Qol. If we compare this figure with ERA40 plots Figure 4.15 and 4.15, we find out that it is the same maximum wind speed recorded during 1960 until 2001, and we can have confidence to our result.

Validation of WAM model collocation

In some areas, altimeter measurements data are the only source of data for model validation. We start by looking at the comparisons between WAM and altimeter significant wave height measurements, the linear regression and density distribution of wave height comparisons between WAM and altimeter in Figure 4.22 clearly appear that our WAM model underestimates the wave heights by 39 cm on average, see Table 4.2. The moderate correlation coefficient (0.72) in Figure 4.22 (a) is mainly due to the coarse wind field used. Small scale wind fields may contain high speed features. Figure 4.26 confirm that wave heights is underestimated by the model. The spatial distribution of the altimeter data, Figure 4.23 (a) shows missing data in many locations because of the fixed repeat orbits of the satellites.

The underestimating of WAM wave height can have something to do with the resolution of the model. If the resolution would have been better, maybe the significant wave height would have been better predicted. As Cavaleri and Bertotti, 2002 [5] found in their study when they start to increase the model resolution it leads to better results. Another thing to notice is that the model is underestimates relatively small waves more than high waves.

Chapter 6

Conclusions

A hindcast of the wave conditions in the Red Sea was made. This has been done by using the WAM model. Results show that in winter time significant wave height can reach 2 m which could be dangerous for small vessels. This study gives some knowledge about the wave conditions in both offshore and coastal regions in the Red Sea, which can help engineers for the design of near shore projects. The quality of the hindcast for the wave height and direction are not bad, but it only gives a rough picture of the sea state. In order to be able to use WAM in scientific matter later on, there has to be some improvement to make the model more accurate. A way to improve the model would be to use higher resolution winds. Observation by waverider buoys in the Red Sea could improve the state of knowledge as well.

Red Sea significant wave height hindcast by the third generation wave model WAM compared with significant wave heights measured by altimeters (GEOSAT FOLLOW-ON, JASON, and INVISAT) for year 2007, produced many features revolved by different analysis techniques. WAM underestimates wave heights for the small waves relatively relatively more than high waves. The correlation between the model results and the altimeter wave heights is more or less good in general.

Appendix A

Model System

A.1 Model System

The model system consists of three major program parts:

1. Pre-processing programs
2. Processing programs
3. Post-processing programs

A.1.1 Pre-processing Programs

Two pre-processing programs are provided:

1. PREPROC
2. PRESET

Program PREPROC
PREPROC generates all time independent information for the wave model.Starting from a regional or global topographic data set, the model grid is created in the form required for the model. The frequency and angular arrays are generated.If the current refraction option is activated, PREPROC expects a current data set and interpolates the data onto the model grid.
A number of model constants are precomputed and stored together with the model grid, frequency and angular information, and the currents in two output files. If

nested grids are generated, the information for the output, input and interpolation of boundary spectra are precomputed and stored in separate files for the coarse and fine (sub) grid models.

Program PRESET
PRESET generates an initial wave field for a wave model cold start. Controlled by the user input of PRESET, either the same initial JONSWAP spectrum is used at all sea points or the initial spectra are computed from the local initial winds according to fetch laws with a cos2 directional distribution. The data are stored in the format of the model restart files.

A.1.2 Processing programs

Two processing programs are provided:

1. CHIEF
2. BOUINT

Program CHIEF
CHIEF is the shell program of the stand-alone version of the wave model calling the subroutine version of the wave model. All time dependent variables and user defined parameters are fixed, the wind fields are transformed into the model formats, and the transport equation is integrated over a chosen period.The program uses the output files of PREPROC as setup files and the files generated by PRESET or a former model run as initial values. A wind input file has to be provided by the user.
All additional information must be defined in the user input file. The model can be integrated with independently chosen propagation, source term, wind input and wind output time steps. However, all time step ratios must be an integer or inverse integer. A number of model options and parameters can be selected by the user in the program input. The following model options are implemented:

- Cartesian or spherical propagation.

- Deep or shallow water.
- Without or with depth or with depth and current refraction.
- Nested grids.
- Time interpolation of winds or no time interpolation.
- Model output at regular intervals or by list.
- Printer and-or file output of individually selected parameters.

All run time dependent files are fetched dynamically and follow a fixed file name convention. The user has control over directory names and paths through the model input.

Program BOUINT
Program BOUINT interpolates the boundary output spectra from a coarse grid model run in time for the fine grid boundary input. This program has to be applied if nested grids are used.

A.1.3 Post-processing programs

Four post-processing programs are provided:

1. PGRID Prints GRIDded output file.
2. PSWGRID Prints SWell GRIDded output file.
3. PSPEC Prints SPECtra output file.
4. PSWSPEC Prints SWell SPECtra output file.

Each of the programs is set up for a model result file. Controlled by the user input the results are printed. Plot software is not included in the standard set of programs. The files are dynamically fetched. The user may choose individual fields. If boundary spectra files are produced, both the course and fine grid file can be printed by program PSPEC.

Appendix B

Examples of WAM input and output files

Binary forcing data files

Wind input file, topography input file, and output file with wave parameters are sequential, binary files with a special structure. Necessary preprocessing and post-processing programs are provided so that the wind input and the wave parameter output are reformatted to grib format (Ref. description of `runwam.sh`). However, an overview of the sequential binary file structure may be useful.

The data are given as 16-bits integers (`INTEGER*2` in Fortran). Before each data field there isa 20-word header that describes the field:

```
Number    Description
1         Producer number
2        Grid area number
3        Data type (1 or 3 is analysis, 2 is prognosis)
4        Time parameter (Hours from start of prognosis)
5        Vertical coordinate (1=pressure, 2=sigma, 3=height)
6        Parameter number (not the same parameter no.  as in grib files)
7        Level 1
8        Level 2
9        Gridtype rectangular/geographical (2=lat/long grid)
10        Number of grid points in x-direction / longitude
11        Number of grid points in y-direction / latitude
12        Year
13        Month*100+day
14        Hour*100+minute
15        Geogr- Latitude of origin * 100
```

```
16        aphical Longitude of origin * 100
17        grid Grid distance in latitude * 100
18        Grid distance in longitude * 100
19        Not used
20        Scaling factor E. All data values are multiplied by 10**E
```

Then follow the data for the first latitude, data for the second latitude and so on.

Some parameter numbers:

```
33 :  u (east to west) component of wind.
34 :  v (south to north) component of wind.
200 :  Significant wave height total sea
201 :  Peak period total sea
201 :  Mean period total sea
203 :  Peak direction total sea
204 :  Mean direction total sea
210 :  Hs wind sea
211 :  Peak period wind sea
212 :  Peak direction wind sea
213 :  Mean period wind sea
214 :  Mean direction of wind sea
220 :  Hs swell
221 :  Peak period swell
222 :  Peak direction swell
223 :  Mean period swell
224 :  Mean direction swell
```

Appendix C

Matlab code used to extract information from WAM output

This appendix provides the MATLAB code that was used to extract the information from WAM output data for the four fishing grounds .

C.1 Matlab code

```
%%%%%%%%%%%%%%%%%%%%%%%%
% Port Sudan                    %
%%%%%%%%%%%%%%%%%%%%%%%%
```

Here you can select the variable significant wave height, speed and wind direction from WAM result, and make what you want of plots like time series and show the correlation between wind speed and wave height

```
function [speed,day,dir,swh]=Time_series_01;
```

%Input file

```
ps=load('wam_67_134_portsudan_01.txt');
```

%Total number of cases

```
N=3969;
```

%Number of days for the month

```
nday=31;  dt=3/24;
day=dt:dt:nday;
```

%Output file

```
fid=fopen('wam_67_134_portsudan_01_new.txt','w');
```

%In this file there are many parameters and just we need sig. wave height(200), wind speed(298) and wind direction(299)

```
wh=0;    wp=0;    wd=0;
for i=1:N;
if ps(i,7)==200;
wh=wh+1;
swh(wh)=ps(i,9);
end;
if ps(i,7)==298;
wp=wp+1; speed(wp)=ps(i,9);
end;
if ps(i,7)==299;
wd=wd+1; dir(wd)=ps(i,9); end;
end;
x=0.125;
for k=1:nday*8;
```

```
fprint(fid,'%6.3f  %6.3f  %6.3f  %6.3f  \n',day(k),speed(k),dir(k),swh( k));
end;
fclose(fid);
```

```
%Time series plot
figure; plotyy(day,swh,day,speed);
xlabel('Time .(days)','fontsize',13);
set(gcf,'color',[1 1 1]);grid on
```

```
%Wind rose plot
dnew=mod(-90-dir,360) ;
figure
handles = wind_rose(dir,speed,'di',[0 2 4 6 8 10 12]);
```

C.2 Statistics

Mean:

$$mean = \frac{\sum_{i=1}^{N} X_i}{N} \tag{C.1}$$

Root mean square error,rms:

$$rms = \sqrt{\frac{\sum_{i=1}^{N} (X_i - Y_i)^2}{N}} \tag{C.2}$$

Standard deviation:

$$Std.\ dev. = \sqrt{\frac{\sum_{i=1}^{N} \left(X_i - \bar{X}\right)^2}{N-1}} \tag{C.3}$$

Appendix D

Additional figures

This appendix provides some additional figures and their description that are not fully described in Chapter 4.

Suakin wind speed, wave height, and wind direction:

Figure D.1 illustrates time series of wind speed and wave height at Suakin and it seems to be the same figure as in Figure 4.6 but it is not, this similarity came from the relative distance between two location and due to the same season. Maximum wave height is about 2 m recorded at the end of day 04.01.2007 corresponding with the maximum wind speed about 12 ms^{-1} recorded earlier at the beginning of 04.01.2007.

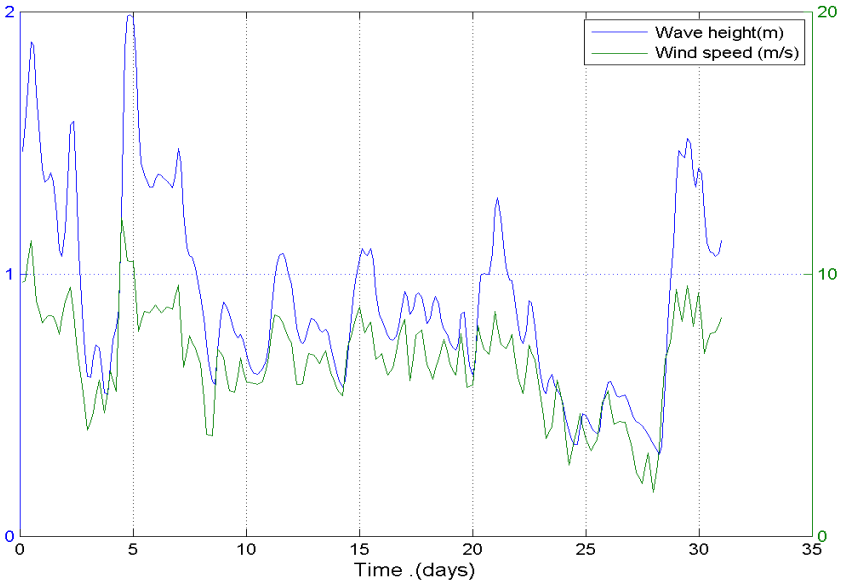

FIGURE D.1: Time series of wind speed and wave height at Suakin , January 2007.

Figure D.2 shows January wind rose for Suakin 2007, based on 31 days of every three hours wind data. This rose shows that the winds was blowing from the north west most of time same as what we present in Port Sudan. The spikes around the north west direction comprise about 74% of all 3 hour wind directions.

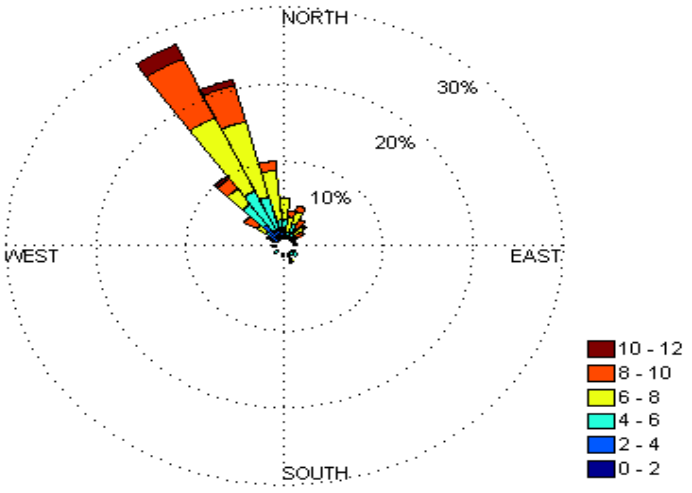

FIGURE D.2: Wind rose plot shows wind direction at Suakin during January 2007.

Histograms of wind speed in Port Sudan and Moh. Qol:

The wind speed in the Red Sea varies according to the season. Figure D.3 shows a histogram plot of the wind speed in the Red Sea during the whole 2007. In (a) Port Sudan, we see that the speed varies between 0 and 13 ms^{-1}. Only in few cases the wind speed is larger than 10 ms^{-1}. In (b) Moh. Qol, the speed variation is between 0 and 12 ms^{-1}.

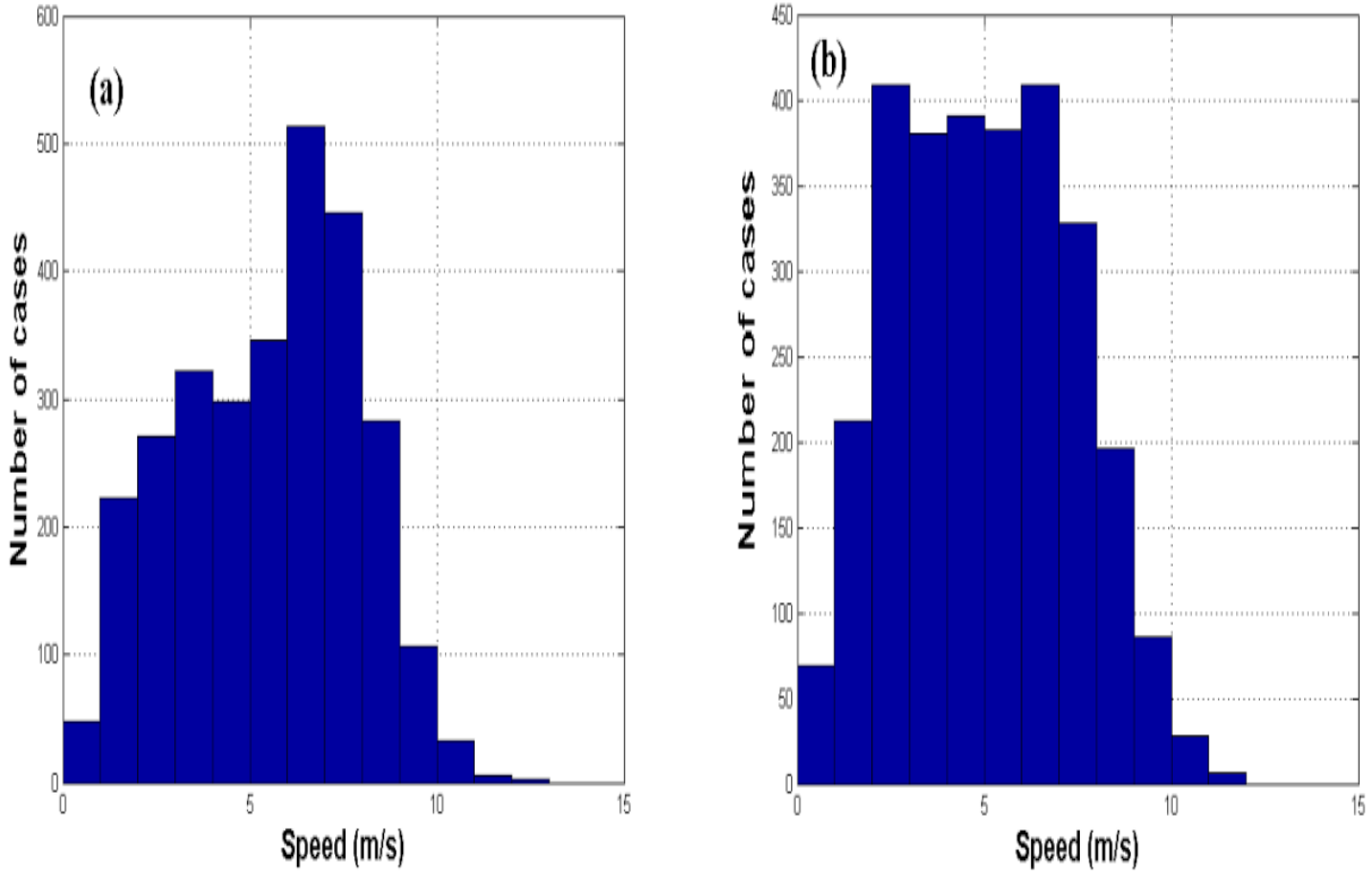

FIGURE D.3: Histogram of wind speed in the Red Sea for the whole 2007, (a) Port Sudan and (b) Moh. Qol.

Histograms of wind speed in Suakin and Middle of the Red Sea:

Figure D.4 illustrates a histogram of significant wave height in Suakin and middle of the Red Sea. In Suakin the maximum wave height was less than 2 m during 2007, but vary between 0.1 and 1.99 m. Most dominant wave height is between 0.6 and 1 m. In the middle of the Red Sea; Figure D.4 (b) the wave height exceed 2 m in a few cases and the maxima here is about 2.25 m. The variation of the wave height in this area is between 0.125 and 1 m.

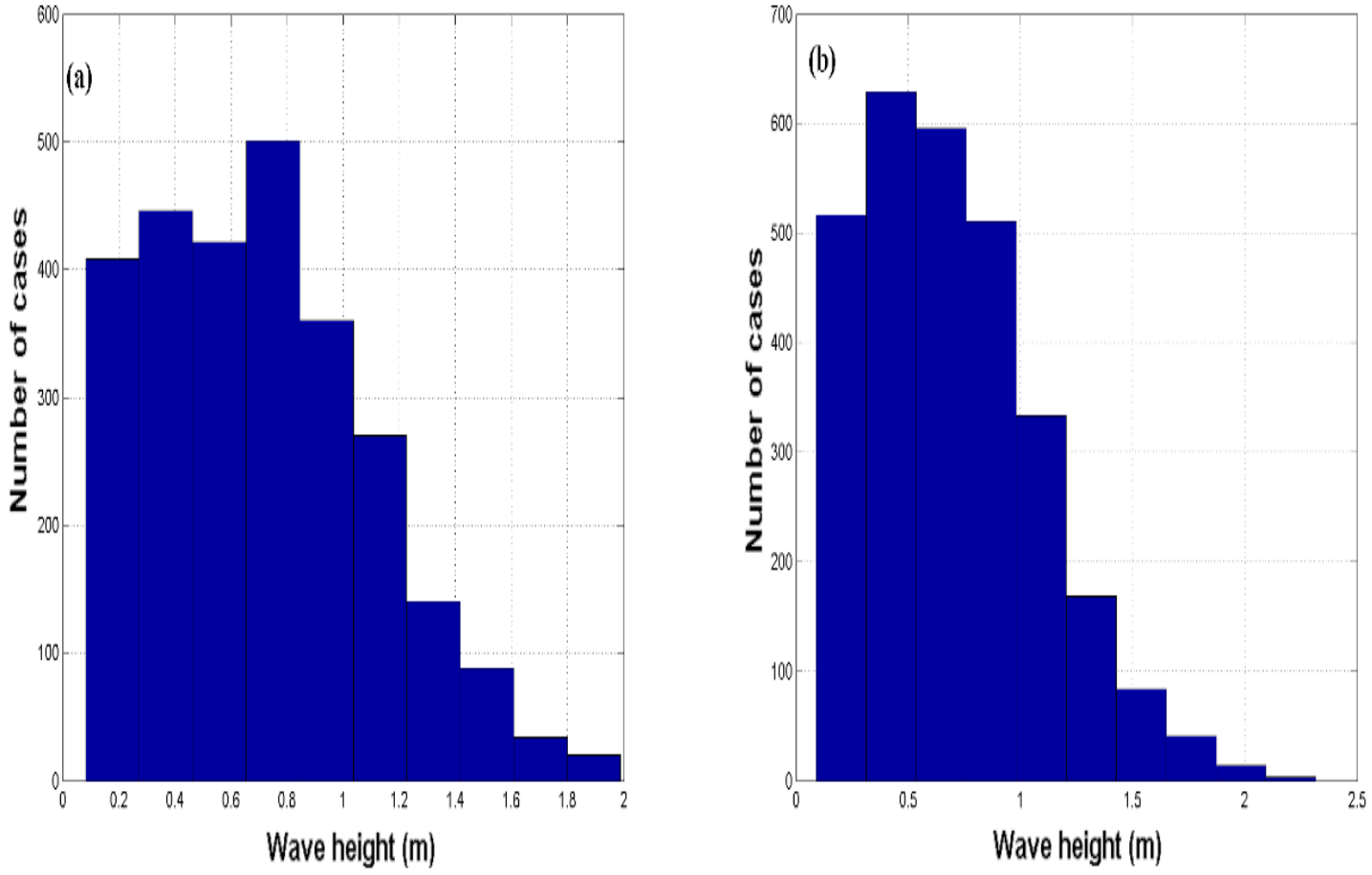

FIGURE D.4: Histogram of significant wave height in the Red Sea for the whole 2007, (a) Suakin and (b) Middle of the Red Sea.

When comparing the two figures we see that in the middle of the Red Sea there is a few cases where wave height exceed 2 m which make sense because this

area in the open sea. In general there is much variation in Suakin than in the middle of the Red Sea.

References

[1] John Pike , The Federation of American Scientists. Geosat follow-on [gfo]. http://www.fas.org/spp/military/program/met/gfo.htm, 25 May 2010.

[2] HowStuffWorks 30 March 2008. The red sea. http://geography.howstuffworks.com/oceans-and-seas/the-red-sea.htm, 29 October 2009.

[3] Kraaiennest. Wikimedia Foundation Inc .18 April 2008. Dispersion (water waves). http://en.wikipedia.org/wiki/Red_Sea#cite_note-1, 15 November 2009.

[4] Elsheikh Bashir Ali. The inorganic carbon cycle in the red sea. Master's thesis, [E.B. Ali], 2008. Mastergradsoppgave (M.Sc.) i kjemisk oseanografi - Universitetet i Bergen, 2008 I.

[5] LUIGI CAVALERI and LUCIANA BERTOTTI. Accuracy of the modelled wind and wave fields in enclosed seas. *Tellus A*, 56(2):167–175, 2004.

[6] Alasdair J. Edwards, Stephen M. Head, International Union for Conservation of Nature, and Natural Resources. *Red Sea*. Oxford ; New York, 1st edition, 1987.

[7] European Centre for Medium Range Weather Forecasts. Ecmwf newsletter. Description based on: No. 110 (Winter 2006/2007).

[8] Wikimedia Foundation Inc. Waves and the concept of a wave spectrum. http://www.wikiwaves.org/index.php/Waves_and_the_Concept_of_a_Wave_Spectrum, 01 October 2009.

[9] Komen G. J. *Dynamics and modelling of ocean waves*. Cambridge University Press, Cambridge, 1994.

[10] Lighthill M. J. *Waves in fluids*. Cambridge University Press, 1978.

[11] Sofianos S. S. Johns W. E. An oceanic general circulation model (ogcm) investigation of the red sea circulation: 2. three-dimensional circulation in the red sea. *Journal of Geophysical Research-Oceans*, 108(C3), 2003.

[12] NASA JPL and the Texas A & M Department of Oceanography 2004. Chapter 16 - ocean waves. http://oceanworld.tamu.edu/resources/ocng_textbook/chapter16/chapter16_04.htm, 01 October 2009.

[13] Gelci R. H. Cazale and J.Vassal. Previson de la houle. la methode des densites spectroangulaires (prediction of waves . the method of frequency-directional spectral densities). *Bull. Infor. Comite Central Oceanogr*, pages 416–435, 1949.

[14] Hasselmann K. *Measurements of wind-wave growth and swell decay during the Joint North Sea Wave Project (JONSWAP)*. Deutsches Hydrographisches Institut, 1973.

[15] Hasselmann K. The wam model - a 3rd generation ocean wave prediction model. *Journal of Physical Oceanography*, 18(12):1775–1810, 1988.

[16] Yves Ménard, Lee-Lueng Fu, P. Escudier, F. Parisot, J. Perbos, P. Vincent, S. Desai, B. Haines, and G. Kunstmann. The jason-1 mission – special issue: Jason-1 calibration/validation. *Marine Geodesy*, 26(3):131 – 146, 2003.

[17] Pierson W. J. Moskowitz L. Proposed spectral form for fully developed wind seas based on similarity theory of s a kitaigorodskii. *Journal of Geophysical Research*, 69(24):5181, 1964.

[18] Office of Naval Research. Ocean in motion: Waves - characteristics. http://www.onr.navy.mil/Focus/ocean/motion/waves1.htm, 29 October 2009.

[19] McGraw Hill Encyclopedia of Science and Technology 1997. Wave (physics). http://www.accessscience.com,DOI10.1036/1097-8542.740200, 19 October 2009.

[20] Aarnes Ole Johan. On mixed wind-sea/swell conditions in the open ocean: model and radar-observations. Master's thesis, 2005.

[21] World Meteorological Organization. *Guide to wave analysis and forecasting*. Secretariat of the World Meteorological Organization, Geneva, 1998. 2nd ed.

[22] Pinet Paul R. *Invitation to oceanography*. Jones and Bartlett Publishers, 3rd edition, 2003.

[23] Mississippi C. Linwood Vincent Ph.D., Zeki Demirbilek Ph.D. Coastal, Engineer Research Hydraulics Laboratory (CHL), Development, and Office of Naval Research Arlington Virginia. Center, Vicksburg. *Coastal Engineering Manual - Chapter 1 Part II*. 2008.

[24] Queffeulou Pierre. Long-term validation of wave height measurements from altimeters. *Marine Geodesy*, 27(3):495 – 510, 2004.

[25] Kundu Pijush K. *Fluid mechanics*. Academic Press, San Diego, Calif., 1990.

[26] A. Resti, J. Benveniste, M. Roca, G. Levrini, and J. Johannessen. The envisat radar altimeter system (ra-2). *Esa Bulletin-European Space Agency*, (98):94–101, 1999.

[27] *Ka°llberg* P. Rob Hine, Sylvie Lamy-Thepaut, Simmons Adrian, Hoskins1 Brian, Berrisford1 Paul, and Uppala Sakari. Era-40 atlas. european centre for medium range weather forecasts. 2005.

[28] Rosmorduc, V., J. Benveniste, O. Lauret, C. Maheu, M. Milagro, and N. Picot. Radar altimetry tutorial. http://www.altimetry.info/html/alti/principle/waveform/ocean_en.html, 01 June 2010.

[29] M. R. Tucker and D. E. Pedgley. Summer winds around southern red-sea. *Archiv Fur Meteorologie Geophysik Und Bioklimatologie Serie B-Klimatologie Umweltmeteorologie Strahlungsforschung*, 25(3):221–231, 1977.

[30] S. M. Uppala, P. W. Kallberg, A. J. Simmons, U. Andrae, V. Da Costa Bechtold, M. Fiorino, J. K. Gibson, J. Haseler, A. Hernandez, G. A. Kelly, X. Li, K. Onogi, S. Saarinen, N. Sokka, R. P. Allan, E. Andersson, K. Arpe, M. A. Balmaseda, A. C. M. Beljaars, L. Van De Berg, J. Bidlot, N. Bormann,

S. Caires, F. Chevallier, A. Dethof, M. Dragosavac, M. Fisher, M. Fuentes, S. Hagemann, E. H?lm, B. J. Hoskins, L. Isaksen, P. A. E. M. Janssen, R. Jenne, A. P. Mcnally, J.-F. Mahfouf, J.-J. Morcrette, N. A. Rayner, R. W. Saunders, P. Simon, A. Sterl, K. E. Trenberth, A. Untch, D. Vasiljevic, P. Viterbo, and J. Woollen. The era-40 re-analysis. *Quarterly Journal of the Royal Meteorological Society*, 131(612):2961–3012, 2005. 10.1256/qj.04.176.

[31] Honjo S. Weller R. A. Monsoon winds and carbon cycles in the arabian sea. *Oceanus*, 40(2):24–28, 1997.

[32] Inc. Wikimedia Foundation. Red sea. http://en.wikipedia.org/wiki/Red_Sea#cite_note-1, 09 November 2009.

[33] Pierson Willard J. *Practical methods for observing and forecasting ocean waves by means of wave spectra and statistics*. United States. Hydrographic Office. H.O. pub. Hydrographic Office, [Washington], 1955.